Surface properties of metastable alumina: A comparative study of κ- and α-Al_2O_3

C. Ruberto,[1] Y. Yourdshahyan,[2] and B. I. Lundqvist[1]
[1]*Department of Applied Physics, Chalmers University of Technology and Göteborg University, SE-412 96 Göteborg, Sweden*
[2]*Department of Chemistry and Laboratory for Research on the Structure of Matter, University of Pennsylvania, Philadelphia, Pennsylvania 19104-6323*
(Received 6 August 2002; published 30 May 2003)

First-principles calculations are performed on the stable α-Al_2O_3 and metastable κ-Al_2O_3 phases to understand the stability and bonding of the flexible alumina surfaces. The (001) and $(00\bar{1})$ surfaces of κ-Al_2O_3 are investigated and compared to α-$Al_2O_3(0001)$. A needed extension of the original formulation of the Tasker's rule for the stability of low-symmetry ion-crystal surfaces is found. Also, use of extended Pauling's rules makes the results applicable to other metastable alumina phases. The most stable termination of $\kappa(001)/(00\bar{1})$ is found to be in the middle of an Al layer, similarly to α-$Al_2O_3(0001)$. This surface is shown to be nonpolar, even though a Tasker point-charge description implies a polar classification. The asymmetry in atomic and electronic structures introduced by the tetrahedrally coordinated Al (Al^T) ions is found to have important consequences for the surface properties. The bulk cation-vacancy lines caused by the Al^T make the $\kappa(001)/(00\bar{1})$ surfaces more open than $\alpha(0001)$, thus allowing a huge inward relaxation (-117%) at $\kappa(001)$, making this surface O terminated. The charge asymmetry in bulk κ-Al_2O_3 causes an excess of electrons at $\kappa(00\bar{1})$, yielding a one-dimensional metallic surface state. Also, the presence of Al^T in the near-surface layer is found to be destabilizing.

DOI: 10.1103/PhysRevB.67.195412 PACS number(s): 68.35.Md, 73.20.At

I. INTRODUCTION

Aluminum oxide or alumina (Al_2O_3) is a highly studied metal oxide. It is a scientifically puzzling ceramic with a wide range of applications and a large amount of structural freedom, with phase transitions between many different structures (α, γ, η, θ, δ, κ, χ, ...) occurring at relatively high temperatures.[1] Properties such as high hardness, good mechanical, thermal, and chemical resistances, high electrical resistivity, useful optical properties, fine particle size, high surface area, and catalytic surface activity make the different alumina phases highly useful as, e.g., coatings, substrates, catalysts, catalyst carriers, adsorbents, and soft abrasives; for instance, the stable α phase (sapphire or corundum) in electronics, the γ phase in catalysis, and the κ phase in wear-resistant coatings on cemented-carbide cutting tools.[2,3]

Despite a large amount of efforts at understanding the properties of the alumina phases, many questions still remain unanswered, especially at the fundamental atomistic level, including their crystal structures, their stability and bonding nature, and their phase transformation mechanisms. In particular, a good theoretical description and understanding of the stability properties, considering the fascinating structural flexibility, is desirable. Also, an understanding of surface properties such as atomic and electronic structures and chemical activity is of high interest, particularly in view of the technological importance of the alumina surfaces.

To date, the most studied phase of Al_2O_3 is the stable α phase. This is presumably due to the stability and the less complex structure of this phase, as compared to the metastable aluminas. In spite of their technological relevance, a fundamental understanding of the properties and the stability of the metastable aluminas is still largely lacking. Experimentally, investigations on metastable aluminas are hampered by metastability, poor crystallinity, difficulty in obtaining pure-phase samples, and possible surface-energy stabilization. At the same time, theoretical investigations are made difficult by the need for a high accuracy to describe the small energy differences occurring between the many and often very similar structural possibilities.[4,5] Simple semiempirical methods have shown to be inadequate,[4] which makes first-principles methods at the quantum-mechanical level invaluable tools. However, relatively complex atomic structures[1] make the first-principles methods computationally demanding, putting limits on the applicability of such methods for metastable aluminas.

Because of this, there is still a lack of uncontroversial structural information on the metastable aluminas, which renders accurate theoretical studies on their properties hard to perform. For instance, several metastable aluminas, including the technologically important γ and η phases, are reported to have a disordered Al-sublattice structure, while for others even the form of the crystal unit cell is controversial.[1] Also, the presence of hydrogen in the bulk structure has not been unequivocally ruled out for all phases, for instance, for γ-Al_2O_3 a large number of contradictory results has been published.[6]

However, the presence of tetrahedrally coordinated Al atoms (Al^T) in the structure appears to be common to all or to most of the metastable phases,[1] as opposed to the stable α phase, which has only octahedrally coordinated Al atoms (Al^O). Also, the bonding in all the alumina phases appears to be predominantly ionic. Thus, first-principles investigations on one well-characterized metastable phase can provide general insights into the implications of Al^T for the crystal stability and the nature of the ionic bonding of metastable aluminas. To this end, it is important to analyze the applicability

on the low-symmetry metastable aluminas of intuitive rules for ion-crystal bulk and surface stability, like Pauling's and Tasker's rules, respectively. In particular, to what extent does the idealized point-charge ionic model implicit in these formulations apply to more complex and low-symmetry ionic structures?

The κ-Al_2O_3 phase, with its recently determined bulk atomic structure,[5,7–9] provides an excellent prototype system for such a study, since (i) it has an ordered structure, making the first-principles methods computationally viable; (ii) it has a moderate amount of Al^T, allowing a study of the structural and bonding effects of the Al^T but at the same time keeping sufficient structural similarity with α-Al_2O_3 to permit comparisons; and (iii) it lacks mirror symmetry, allowing a study of the effects of crystal asymmetry on stability and structure properties of highly ionic crystals.

In the present work, the atomic and electronic structures of the α-$Al_2O_3(0001)$ surface and of the κ-$Al_2O_3(001)$ and $(00\bar{1})$ surfaces that can be obtained from cleavage of the bulk structure are investigated with the first-principles calculations based on the density-functional theory (DFT),[10] which has shown its validity in a number of technologically relevant systems.[11] In a recent paper,[12] we had discussed the structure and stability of these peculiar and complex ionic κ-Al_2O_3 surfaces. Here, the aim is to present in more detail the computational details, all numerical results, and some more detailed background and analysis.

The (001) and $(00\bar{1})$ surfaces of κ-Al_2O_3 are chosen because of their structural similarity with the much-studied basal plane of α-Al_2O_3, (0001). This permits comparisons to be made to understand the role of the bulk-structure Al^T for surface properties and stability. Also, [001] and/or $[00\bar{1}]$ are the favored growth directions of chemical-vapor deposited (CVD) κ-Al_2O_3 in cutting-tool coatings.[13] The study of these surfaces is thus also a first step towards a fundamental understanding of the properties of these coatings and of the mechanisms behind the complex CVD growth process.

Further, it has been reported that ultrathin alumina films on Al(111) and Ru(0001) surfaces adopt a κ-Al_2O_3 structure.[14] Thin alumina films are important in, e.g., heterogeneous catalysis[15] and electronics. In particular, they have been proposed to be used as tunnel barriers in magnetoresistive random access memory.[16] Such applications give further motivation to an understanding of the κ-Al_2O_3 surfaces.

We note finally that, considering the fact that the α-Al_2O_3 surface has been reported to react readily with water,[17] affecting its surface reactivity,[18] a study on UHV κ-Al_2O_3 surfaces yields valuable insights for studying such effects at metastable-alumina surfaces as well.

This paper is organized as follows. In Sec. II, the background to our study is provided. First, the computational method used is presented. Thereafter, the bulk structures of α and κ aluminas are described, followed by an introduction to the empirical ion-stability rules of Pauling and a discussion of their relevance for the alumina bulk structures. Extensions to Pauling's original formulations, important for the analysis of our results, are discussed. Then, the question of surface termination and surface stability of ionic crystals is introduced, in terms of Tasker's rule, and the method used by us for the surface-energy calculations is presented. Section III presents the results from our calculations. First, the results for the α-$Al_2O_3(0001)$ surface are presented and discussed. A good agreement is found with the results from previous investigations. Then, the results for the κ-$Al_2O_3(001)$ and $(00\bar{1})$ surfaces are presented and discussed. The questions of surface cleavage termination, polarity, relaxation effects, and electronic structure are addressed. The results obtained from the first-principles calculations are analyzed in terms of extended Pauling's and Tasker's rules. The applicability of these rules for low-symmetry ionic crystals such as metastable aluminas in general is discussed. Finally, the results are summarized in Sec. IV.

II. BACKGROUND

A. Computational method

The calculations are performed with the plane-wave-pseudopotential-based DFT code DACAPO 1.30 (parallelized over both **k** points and electronic bands).[19] Exchange and correlation are treated with the PW91 generalized-gradient approximation (GGA).[20] [For the α-$Al_2O_3(0001)$ surface the local-density approximation (LDA)[21] is also used.] The Kohn-Sham (KS) wave functions are expanded in plane-wave basis sets, up to a given cutoff value for their kinetic energy, and Vanderbilt ultrasoft pseudopotentials are used to describe the electron-ion interactions.[22] [For the α-$Al_2O_3(0001)$ LDA calculations, norm-conserving pseudopotentials (NCPP) are used.[23]] The Brillouin zone is sampled with the Monkhorst-Pack scheme.[24] Slab geometry and periodic boundary conditions are used in the calculations. The potential discontinuity thus arising from the lack of crystal-inversion symmetry in the κ-Al_2O_3 surface calculations is corrected for with the method of Bengtsson.[25] The atomic relaxations are performed with the modified velocity-Verlet algorithm described in Ref. 5, with varying time steps. For all slabs considered, the relaxations are performed until the remaining forces on each atom are <0.03 eV/Å. From the calculated electron densities, local densities of states (LDOS) are obtained by projecting the calculated KS wavefunctions of the considered energy on the atomic orbitals centered around each atom in the crystal structure. The generated pseudopotentials are tested, showing very good transferabilities compared to all-electron values (with errors in the meV regime).[26]

The lattice parameters and energy difference for bulk α-Al_2O_3 and κ-Al_2O_3 obtained with the pseudopotentials generated by us (Table I) using both the PW91 GGA and the LDA show in both cases the pseudopotentials to be very accurate. Further, the well-known tendency of the LDA to overbind is noticed, with lattice parameters $\approx 1\%$ smaller than the experimental values for both phases. On the other hand, the PW91 GGA yields values slightly higher ($\sim 1\%$) than the experimental ones. Also, our calculated energy difference between bulk κ- and α-Al_2O_3 compares very well with the experimental value of Yokokawa and Kleppa,[30] as well as with the calculated one of Wolverton and Hass.[6]

TABLE I. Our calculated lattice parameters and energy difference of bulk α-Al_2O_3 and κ-Al_2O_3 at 0 K from LDA and PW91-GGA DFT, compared with the experimental values at room temperature (RT) and with the all-electron full-potential (FLAPW) and the pseudopotential (VASP code) DFT calculations of Wolverton and Hass (Ref. 6). The experimental lattice parameters for κ-Al_2O_3 are also extrapolated to 0 K for comparison with the calculated values using the thermal expansion coefficients of Ref. 27.

	Our calculations (0 K)		Experiments (RT)		Other calculations (0 K) (Ref. 6)	
Bulk α-Al_2O_3	(LDA) (Ref. 28)	(GGA)	(Ref. 29)		FLAPW (LDA)	VASP (GGA)
a (Å)	5.091	5.185	5.128		5.071	5.161
ϕ (deg)	55.330	55.125	55.280		55.450	55.270
	Our calculations (0 K)		Experiments (RT)		Experiments (extrapolated to 0 K)	
Bulk κ-Al_2O_3	(LDA) (Ref. 5)	(GGA)	(Ref. 27)	(Ref. 8)	(from Ref. 27)	(from Ref. 8)
a (Å)	4.8041	4.875	4.8351(3)	4.8437(2)	4.831	4.840
b (Å)	8.2543	8.378	8.3109(5)	8.3300(3)	8.300	8.321
c (Å)	8.8785	9.018	8.9363(3)	8.9547(4)	8.923	8.945
	Our calculations (0 K)		Experiments (RT)		Other calculations (0 K) (Ref. 6)	
Bulk energy difference	(GGA)	(LDA)	(Ref. 30)		VASP (GGA)	VASP (LDA)
$\delta E(\kappa-\alpha)$ (eV)	0.09	0.15	0.16		0.08	0.21

For the calculations on the α-$Al_2O_3(0001)$ surface, tests yield a good convergence for a vacuum thickness $L_{vac} = c_\alpha/2$ (where c_α is the height of the α-Al_2O_3 hexagonal unit cell), a plane-wave cutoff $E_{cut}=600$ eV ($E_{cut}=900$ eV in the LDA+NCPP calculations), and a $2\times2\times1$ **k**-point sampling of the Brillouin zone. For the κ-$Al_2O_3(001)/(00\bar{1})$ surfaces, good convergence is reached with $L_{vac}=c_\kappa$ (where c_κ is the height of the orthorhombic κ-Al_2O_3 unit cell), $E_{cut}=400$ eV, and a $4\times2\times1$ **k**-point sampling.

B. Alumina bulk structures

The bulk α- and κ-Al_2O_3 structures are both composed of alternating O and Al planes, perpendicular to the c axis (the [0001] and [001] directions in α and κ, respectively), with O in an almost close-packed stacking ($ABAB$ for α and $ABAC$ for κ) and Al in the resulting interstitial sites.

In α-Al_2O_3 (rhombohedral unit cell, space group $R\bar{3}c$), all Al layers consist of hexagonally arranged atoms, occupying 2/3 of the available octahedral sites (Fig. 1).[29,31] In each layer the Al ions arrange themselves in one of the three types of hexagonal networks, which differ in the position of the vacant octahedral sites (α, β, or γ in Fig. 1). By denoting a layer of octahedral sites between a double AB oxygen layer with the stacking letter C, the α-Al_2O_3 structure can be described by the stacking sequence $Ac^\alpha Bc^\beta Ac^\gamma Bc^\alpha Ac^\beta Bc^\gamma$ along [0001], where capital (small) letters denote oxygen (aluminum) layers and the vacancy position in each Al layer is denoted by the greek superscripts.[32] Due to the electrostatic repulsion arising from the face sharing of Al octahedra

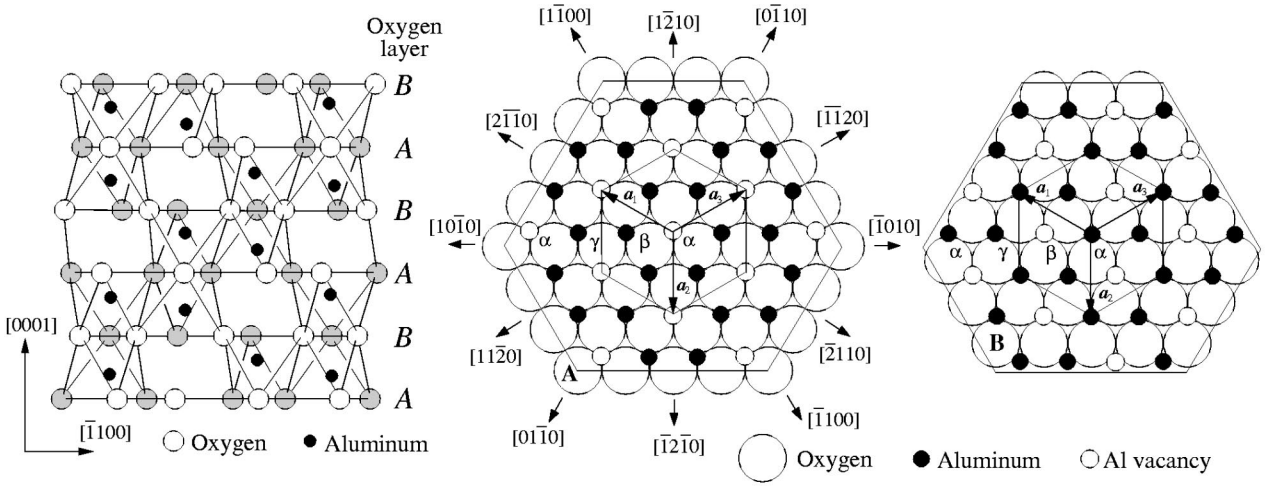

FIG. 1. Bulk structure of α-Al_2O_3. Left: A slice of the structure, one Al-polyhedron thick, showing the stacking sequence along [0001] (''grey'' O atoms are behind the ''white'' ones in the same layer); the Al coordination octahedra are drawn with solid lines. Right: The first two layers of O with Al ions above; vacant Al sites are marked with open small circles; the hexagonal (trigonal) unit cell is shown; α, β, and γ mark the three different Al sites present in the atomic layers of α-Al_2O_3.

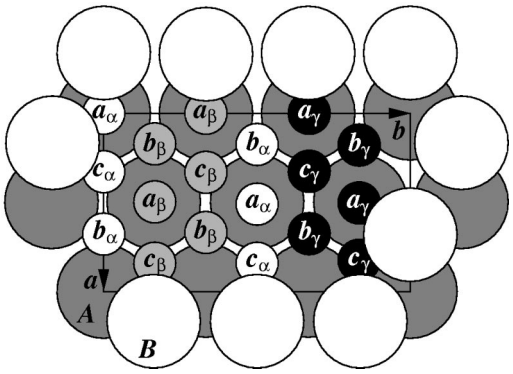

FIG. 2. Notation of the cation positions allowed by the $Pna2_1$ symmetry of κ-Al_2O_3 between two O layers in *A* and *B* stackings. Roman letters denote stacking letter and Greek subscripts denote the three different ion positions allowed for a given stacking letter. Note that, due to the $Pna2_1$ symmetry, the positions are pairwise related within each layer. The in-plane unit cell is marked with solid lines. (From Ref. 5).

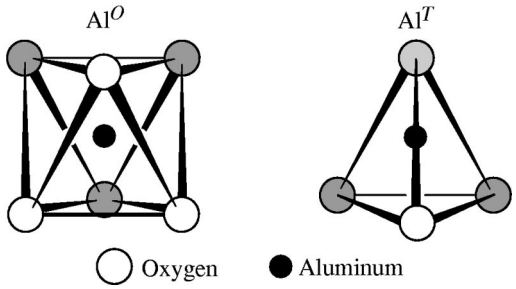

FIG. 3. The two different Al coordinations present in α- and κ-Al_2O_3: octahedral (Al^O) and tetrahedral (Al^T).

in neighboring layers (see the discussion of Pauling's rules in Sec. II C), the Al atoms in each layer are slightly displaced from each other, forming two separate sublayers. All Al layers are thus equivalent to each other, apart from an in-plane displacement of the Al hexagons of one Al^O site in subsequent layers.

On the other hand, in κ-Al_2O_3 (orthorhombic unit cell, space group $Pna2_1$), 3/4 of the Al ions in the unit cell are Al^O and 1/4 is Al^T (Refs. 5,7–9). Using a similar notation as for α-Al_2O_3, introduced in Ref. 5 and reproduced in Fig. 2, the structure of κ-Al_2O_3 can be described as $Ac_\beta b_\gamma Bc_\alpha c_\gamma Ab_\gamma c_\beta Cb_\alpha b_\beta$, where the subscripts now denote the occupied cation positions in each Al layer. Due to the mixture of different Al coordinations in the structure (Fig. 3), there are two different types of Al layers, which alternate along [001] (see Fig. 4): (i) ''octahedral,'' composed of only Al^O, and (ii) ''mixed'' composed of equal amounts of Al^T and Al^O. In the octahedral Al layers, the Al ions are arranged in closely lying pairs of [100] zigzag lines slightly separated along [001], leaving vacancy lines in these layers. In the mixed layers, there are two different types of [100] zigzag lines, one composed of only Al^T and the other of only Al^O. These two lines are homogeneously distributed in the layer and alternate along [010]. Due to their coordination, the Al^T atoms are strongly displaced towards the $[00\bar{1}]$ direction. Also, the O atoms in each layer are separated along [001], due to the Al-sublattice anisotropy.

We note here that, in contrast to α-Al_2O_3, the κ-Al_2O_3 structure lacks mirror symmetry through the (001) plane, making the two (001) and $(00\bar{1})$ surfaces inequivalent. This is due to the presence of Al^T in the structure, together with the fact that their vertices all point towards the [001] direction.

C. Pauling's rules

Based on his experience of structure determination, Pauling put forward his by now classic rules on ion-crystal stability in 1929.[33] The rules summarize efficiently and intuitively the effects of electrostatics and quantum repulsion on ionic-structure stability.

In the case of the alumina structures, rules no. 1, (Ref. 34), 2 (Ref. 35), and 3 (Ref. 36) are the relevant ones. Rule no. 1[34] deals with the issue of the coordination number of the Al cation. Pauling himself concluded that for Al_2O_3 the Al cations can occur in both octahedral and tetrahedral coordinations, his cation-to-anion radius ratio being 0.41. However,

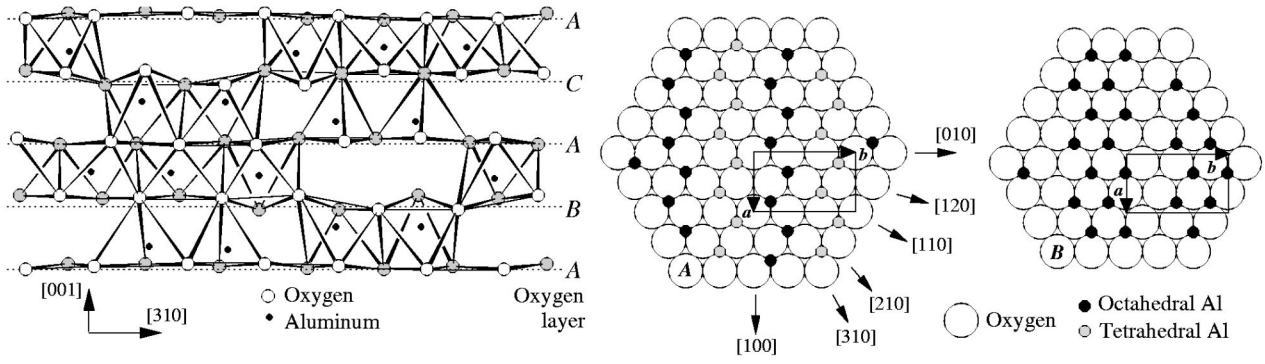

FIG. 4. Bulk structure of κ-Al_2O_3. Left: A slice of the structure, one Al-polyhedron thick, showing the stacking sequence along [001] (''grey'' O atoms are behind the ''white'' ones in the same layer); the Al coordination polyhedra are drawn with solid lines. Right: The first two O layers of the unit cell, with Al overlayers. The in-plane unit cell is shown with solid lines. (From Ref. 5). The crystallographic directions have been corrected, compared to Ref. 5.

use of radius values based on larger structure databases yields that octahedral coordination is favored. Use of the ''crystal radius'' values of Shannon (see Table I in Ref. 37) yields ratios of 0.42–0.43 for Al^T and 0.54–0.56 for Al^O, where the variations depend on the coordination number of the nearest-neighbor O ion. Indeed, this is confirmed by the fact that the stable α-Al_2O_3 phase has only Al^O, while the metastable alumina phases are all known or supposed to have varying amounts of Al^T in their structures [25% in κ-Al_2O_3,[5] 50% in θ-Al_2O_3,[38] and (25–37.5)% in the spinel aluminas (γ-, η-, and δ-Al_2O_3)[6]].

Rule no. 2 (Ref. 35) describes how the cations should be distributed in the structure and, in fact, it is exactly fulfilled in the case of α-Al_2O_3. Our work on κ-Al_2O_3 has shown, however, that its applicability is more limited in the case of metastable aluminas. For example, it was not possible to reproduce the calculated relative stability of the 60 structural candidates for bulk κ-Al_2O_3 (Ref. 5) on the basis of this rule alone. Also, the compliance of the obtained lowest-energy candidate to this rule is limited.

The second rule can, however, be put in a more useful form by using the extension suggested by Brown *et al.*[39] As in Pauling's formulation, the ionicity V_j of an atom j is still given by the sum of the bond strengths s_{ij} between it and its nearest-neighbor atoms i,

$$V_j = \sum_i s_{ij}. \tag{1}$$

According to Brown, however, the bond strength is defined as

$$s_{ij} = \exp\left[\frac{r_0 - r_{ij}}{B}\right], \tag{2}$$

which follows semiempirical and quantum-mechanical arguments.[40] The parameters r_0 and B are fitted to known structural data (for Al–O bonds $r_0 = 1.651$ Å, while $B = 0.37$ is a universal constant), while r_{ij} is the distance between atoms i and j. In this way, the effect of varying cation-anion distances is taken into account (the larger the distance, the weaker the bond strength), thus allowing distortions of the ion coordination polyhedra. This should obviously be very important in such a distorted structural environment as that of κ-Al_2O_3. In Sec. III B, we show that Brown's rule yields atomic ionicities for bulk κ-Al_2O_3 that are very close to those obtained from our DFT calculations. Brown's definition of bond strength should thus yield a very good estimate of the actual amount of electrons donated by a cation to its nearest-neighbor anions in a distorted structural environment.

Interestingly enough, rule no. 3 (Ref. 36) is rather badly fulfilled in α-Al_2O_3. Due to the fact that all Al are Al^O, face sharing between the Al coordination polyhedra cannot be avoided. Apparently, a tetrahedral coordination is more destabilizing than the presence of face sharings (rule no. 1 is more important than rule no. 3). As soon as Al^T are present, however, face sharing can be avoided, simply due to the fact that a tetrahedron has fewer faces to share than an octahedron. In particular, it has only one face in common with one of the two neighboring Al layers. In the κ-Al_2O_3 structure, the vacancy lines in the octahedral layers are located right beneath the Al^T lines in the next layer, thus avoiding face sharing with the Al^T. In the octahedral Al layer above the Al^T, on the other hand, the two Al^O lines are positioned above the Al^T, which does not imply face sharing thanks to the presence of screening O ions in between the two Al layers. Therefore, the κ-Al_2O_3 structure, although it does not fulfill rule no. 1, can still be expected to be rather stable, thanks to rule no. 3, which is probably the reason for its high transition temperature to α-Al_2O_3, at $\sim$1000°C.

It is interesting to note that the same stabilizing interplay between Pauling's first and third rules seems to be at work in other metastable aluminas as well. For example, both the known θ-Al_2O_3 structure and the proposed cubic spinel structures of γ-, η-, and δ-Al_2O_3 (as long as only ideal spinel sites are occupied), all have the Al^T arranged in such a way that Al face sharing is avoided.

The presence of Al^T in the bulk structures thus creates relatively large vacancy regions in the Al layers, close to the bottom triangles of the neighboring Al^T tetrahedra, making these metastable-alumina structures more open than α-Al_2O_3. As shown in Sec. III B, this has very important consequences for their surface stability and structure.

D. Tasker's rule

The creation of a surface in an ionic crystal raises the question of the chemical composition of the surface termination. The electrostatic interactions in ionic compounds have a long-range nature. Thus, the created surface, a major defect in the stable bulk structure, introduces significant effects in the overall stability of the now semi-infinite crystal. On the basis of a simple point-charge model, Tasker[41] analyzed this effect and categorized the ionic surfaces into three groups.

The first two groups describe the ''nonpolar'' surfaces, in which each repeat unit used to build up the semi-infinite crystal has no dipole moment perpendicular to the surface. This can arise either if each atomic layer is electrically neutral (''Tasker type 1''), or, if this is not the case, if the anions and cations are arranged in a symmetrical way in the repeat unit (''Tasker type 2''). For example, NaCl(100) belongs to type 1, since each NaCl(100) atomic layer consists of equal amounts of cations and anions that have the same charge magnitude ($+1$ and -1, respectively). The α-Al_2O_3(0001) surface, on the other hand, is built up of alternating layers of only anions or cations. However, the ion distribution along [0001] is such that there exists a repeat unit that has no net dipole moment (see Fig. 5), making this a type-2 surface. In reality, charge is distributed over the region around the ionic core, but as long as a symmetric environment such as the one in α-Al_2O_3 is considered, the point-charge approximation is reasonable. According to Tasker, nonpolar surfaces are stable. Therefore, he predicts that the clean unreconstructed α-Al_2O_3(0001) surface should be terminated by half an Al layer.[42]

The third of Tasker's groups of ionic surfaces comprises the ''polar'' surfaces.[43] Here, the repeat unit has a dipole

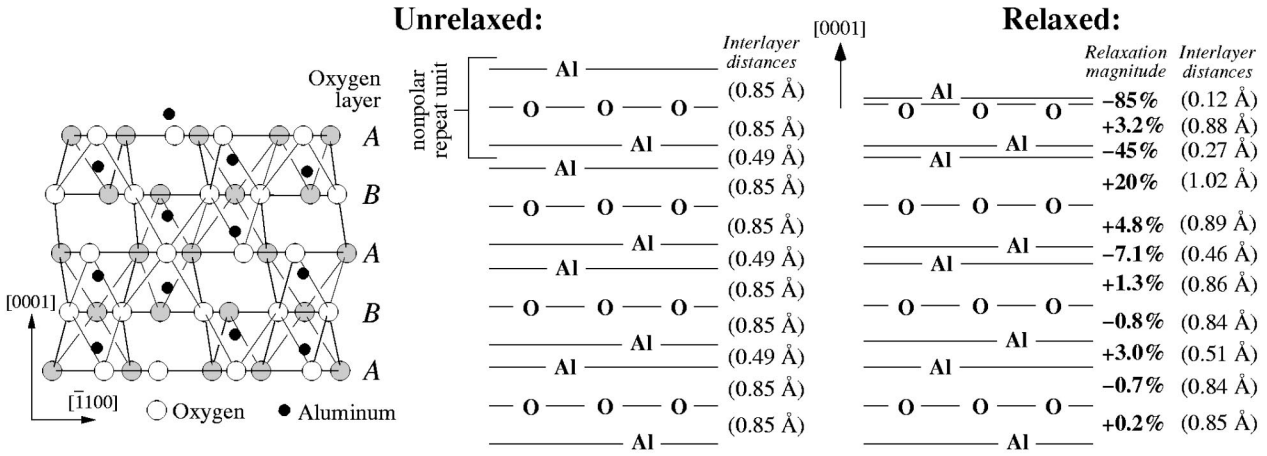

FIG. 5. Nonpolar surface structure of unreconstructed α-$Al_2O_3(0001)$, before and after relaxation, according to our DFT-GGA calculations. The atomic layers perpendicular to [0001] are shown, together with interlayer distances. The relaxation magnitude is given in percentage. The nonpolar repeat unit for building the surface is shown.

moment perpendicular to the surface. This can arise for essentially two reasons. Either the charges on the ionic layers are different from what is needed for a zero dipole moment, such as in NaCl(111), where filled close-packed layers composed of exclusively anions or cations alternate along [111], or there is a symmetrical charge distribution between the atomic layers of the repeat unit *but* the interlayer distances are not symmetrical around the middle plane of the repeat unit. This is the case for κ-$Al_2O_3(001)$ and $(00\bar{1})$. As shown in Fig. 6, the two repeat units (due to the lower symmetry of κ-Al_2O_3, only every second Al layer is equivalent, yielding two different repeat units) that most resemble the $\alpha(0001)$ repeat unit should give polar surfaces, since the interlayer Al–O distances are unsymmetrical.

Thus, *none* of the conceivable terminations that can be obtained from a (001) cleavage of the κ-Al_2O_3 bulk structure is nonpolar. This raises the question on whether this surface actually exists, since, according to Tasker, polar surfaces are electrostatically unstable, having a surface energy that diverges with increasing thickness of the atomic slab. As shown in Fig. 6, there are ten possible cleavage surface terminations. In Sec. III B, the results from our calculations on all of these terminations are reported and put in the context of Tasker's rule.

E. Surface-energy calculations

Our DFT calculations employ a ''slab geometry;'' the surface is described by a supercell composed of a thin film of the crystal (the ''slab'') and a surrounding vacuum region. The slab is composed of a moderate amount of structural units (or ''repeat units''). In order to compare the stability of different surfaces or of different terminations of a surface, the ''surface energy'' is often considered, i.e., the energy cost of producing the surface from an infinite crystal. However, in reality, it is more realistic to talk of a ''cleavage energy,'' or *separation energy* E_{sep}, that is, the amount of energy needed to cleave the infinite crystal and separate the two resulting half infinite crystals from each other.

In a slab calculation, in which the slab composition is stoichiometric, this separation energy corresponds to the sum of the surface energies of the two slab surfaces. It can be obtained as

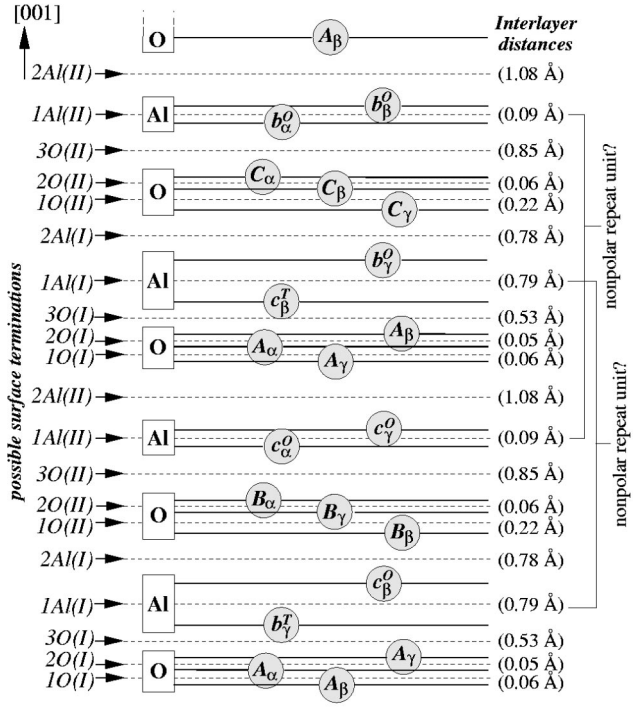

FIG. 6. Bulk structure of one κ-Al_2O_3 unit cell, schematically shown by the stacking of atomic layers along [001]. Each atomic pair in the layers is denoted by the position notation of Fig. 2. To the right, the two repeat units most resembling the repeat unit of the nonpolar α-$Al_2O_3(0001)$ surface are marked. To the left, all the ten nonequivalent (001) cleavage planes of the κ-Al_2O_3 structure are shown and labeled. Note that, due to the $Pna2_1$ symmetry of the κ-Al_2O_3 structure, each atomic layer n is symmetry related to layer $n+2$ (Ref. 5), making cleavage at layer n equivalent to cleavage at layer $n+2$.

TABLE II. Calculated surface energy E_s for the unrelaxed nonpolar α-$Al_2O_3(0001)$ surface as a function of the number of repeat units n in the slab, using the method described in Sect. II E. For each value of n, E_{cell} is the calculated total energy of the whole supercell, E_b is the bulk binding energy of one repeat unit obtained from Eq. (4), and E_s is obtained from Eqs. (3) and (5).

	LDA:		
n	E_{cell} (eV)	E_b (eV)	E_s (J/m^2)
3	−4273.1512		
4	−5700.7333	−1427.5821	3.9707
5	−7128.3179	−1427.5846	3.9748
6	−8555.8992	−1427.5813	3.9680
7	−9983.4772	−1427.5780	3.9598
8	−11 411.0608	−1427.5836	3.9760
9	−12 838.6435	−1427.5827	3.9730
10	−14 266.2226	−1427.5791	3.9596
	Average:	−1427.5816	3.9696
	GGA:		
n	E_{cell} (eV)	E_b (eV)	E_s (J/m^2)
3	−4933.5961		
4	−6581.0976	−1647.5015	3.5790
5	−8228.6033	−1647.5057	3.5858
6	−9876.1082	−1647.5049	3.5842
7	−11 523.6125	−1647.5043	3.5827
8	−13 171.1131	−1647.5006	3.5723
9	−14 818.6230	−1647.5099	3.6022
10	−16 466.1234	−1647.5004	3.5678
	Average:	−1647.5042	3.5827

$$E_{sep} = E_{cell}(n) - nE_b, \tag{3}$$

where $E_{cell}(n)$ is the calculated total energy of a slab with n repeat units and E_b is the bulk binding energy of one repeat unit.

The bulk energy E_b can be obtained from a separate bulk calculation of the crystal. However, such an approach has been shown to yield a separation energy that diverges with increasing slab thickness.[44,45] Therefore, we choose here the more consistent approach of calculating the bulk binding energy as[46]

$$E_b = E_{cell}(n) - E_{cell}(n-1). \tag{4}$$

At sufficiently large n, this value converges, apart from oscillations arising from quantum-size effects (QSE),[47,45] thus ensuring the convergence of E_{sep}.

If the two slab surfaces are equivalent, as in α-$Al_2O_3(0001)$, the surface energy E_s can then be obtained as

$$E_s = E_{sep}/2. \tag{5}$$

For nonequivalent surfaces, as in κ-$Al_2O_3(001)/(00\bar{1})$, only E_{sep} can be extracted.

Table II shows our results for the unrelaxed α-$Al_2O_3(0001)$ surface, using both LDA and GGA. Up to ten repeat units (each consisting of one oxygen layer) are considered. Oscillations from QSE are visible and in the range of ± 0.02 J/m^2 for the surface energy. The surface energy is well converged for $n=4$, implying that without relaxation effects, a three-layer slab is sufficient for obtaining two independent slab surfaces. For the relaxed surface, on the other hand, $n \geqslant 5$ is needed for convergence, due to the long-ranged surface relaxations.

Our results for the unrelaxed κ-$Al_2O_3(001)$ and $(00\bar{1})$ surfaces, using the GGA, also show good convergence of E_b and E_{sep} at $n=4$, where, however, each repeat unit is now composed of two oxygen layers. For the relaxation of the (001) surface, good convergence is still maintained at $n=4$, while $n=5$ is needed for the $(00\bar{1})$ surface, which undergoes a much deeper relaxation. QSE oscillations of about ± 0.02 J/m^2 for the separation energy can be seen in the calculated values.

III. RESULTS AND DISCUSSIONS

A. α-$Al_2O_3(0001)$

For at least the last 15 years, the unreconstructed clean α-$Al_2O_3(0001)$ surface has been the subject of theoretical studies. However, only recently, a clear and consistent description has emerged, thanks also to the contribution of experiments. It is now known that there are large and deep relaxation effects of the surface and that calculations need thick slabs to account for this. The first thick-slab first-principles calculation on (0001) was performed by Verdozzi *et al.*[48] in 1999 on slabs of 9 and 18 repeat units using DFT-LDA. Significant relaxations were found to occur as far as in eight repeat units into the bulk. The large inward relaxation found for the surface Al layer (-87.4%) is attributed to the high ionicity and small radius of the Al^{3+} ion,[48] together with the fact that the open structure of α-Al_2O_3 (with vacancies directly beneath the surface Al ions, see Fig. 5) allows a large inward relaxation while conserving nearest-neighbor bond lengths.[51] The energy gain of the relaxation is calculated to be 0.13 $eV/Å^2 = 2.08$ J/m^2 (Ref. 48). Also, for the unrelaxed surface, this and previous tight-binding calculations[51] report the presence of an Al surface state in the band-gap region. The relaxation drives this state up in energy towards the bottom of the conduction band.

The nature of the surface termination has also been studied theoretically. As discussed in Sec. II D, Tasker's rule predicts that the most stable surface is terminated by half an Al layer. Results of the first-principles calculations on the clean surface agree with this.[52,53] Further, recent investigations on the stability of the surface in an environment of varying oxygen pressure show this termination to be very stable even at high O partial pressure.[54–57]

In order to assess the accuracy of our method, as well as for subsequent comparison to the κ-$Al_2O_3(001)/(00\bar{1})$ system, we perform new LDA and GGA calculations on the clean nonpolar α-$Al_2O_3(0001)$ surface and compare our results to the previously published ones. In addition, we per-

TABLE III. The relaxation of the outermost atomic layers of the unreconstructed nonpolar α-$Al_2O_3(0001)$ surface, as obtained from our DFT-LDA and DFT-GGA calculations on a slab with nine repeat units (see also Fig. 5).

	LDA		GGA	
	(%)	(Å)	(%)	(Å)
Al–O	−85.7	−0.712	−85.5	−0.727
O–Al	+3.5	+0.029	+3.2	+0.027
Al–Al	−43.9	−0.214	−45.4	−0.223
Al–O	+20.0	+0.166	+19.8	+0.168
O–Al	+5.5	+0.046	+4.8	+0.041
Al–Al	−8.6	−0.042	−7.1	−0.035
Al–O	+2.0	+0.017	+1.3	+0.011
O–Al	−0.5	−0.004	−0.8	−0.007
Al–Al	+3.0	+0.015	+3.0	+0.015
Al–O	−0.4	−0.004	−0.7	−0.006
O–Al	+0.6	+0.005	+0.2	+0.002
Al–Al	−0.4	−0.002	−0.3	−0.001
Al–O	+0.8	+0.006	+0.4	+0.004

form a comparison between the accuracies of the LDA and the GGA for the α-$Al_2O_3(0001)$ surface.

Table III shows our calculated surface relaxation. A very good agreement between the LDA and the GGA results is observed, with the largest difference, 0.015 Å, occurring for the top interlayer distance. Also, our nine-layer calculations agree well with the previous LDA results of Verdozzi *et al.*[48] on an eighteen-layer slab (top-layer relaxations of −87.4%, +3.1%, −41.7%, and +18.9%), as well as with the more recent ones obtained with the VASP code by Siegel *et al.*[49] using both the LDA and the GGA (−83%, +3%, −46%, and +19%) and by Gomes *et al.*[50] using the GGA (−86%, +4%, −48%, and +21%). Use of the LDA is thus sufficient for surface calculations on α-Al_2O_3. Also, as already pointed out by Verdozzi *et al.*,[48] a nine-layer slab is found sufficient for a good description of the relaxation effects.

Table IV lists our calculated surface energies E_s showing again a good agreement with the result of Verdozzi *et al.*

TABLE IV. Surface energy of the nonpolar α-$Al_2O_3(0001)$ surface, as obtained from our DFT-LDA and DFT-GGA calculations. The values for both unrelaxed and relaxed surfaces are shown, as well as the energy gain of relaxation. The latter is compared to the value of the DFT-LDA calculation of Verdozzi *et al.* (Ref. 48). Also shown are the values obtained by correcting our LDA and GGA values with the correction term of Mattsson and Jennison (Ref. 60). All values are in J/m^2.

	Unrelaxed	Relaxed	Gain
LDA	3.97	1.94	2.03
GGA	3.58	1.60	1.98
Verdozzi *et al.* (Ref. 48) (LDA)			2.08
LDA + correction	4.25	2.22	2.03
GGA + correction	4.21	2.23	1.98

However, while there is a good agreement between the LDA and the GGA for the value of the energy gain of relaxation, a significant difference is observed for the E_s values. This raises a question on the accuracy of the functionals for the description of the alumina surfaces. In reality, the strong electron-density variations occurring in a surface region call for the truly nonlocal density dependence of the exchange-correlation effects to be accounted for beyond the both local (LDA) and semilocal (GGA) approximations.[58–60] Since the surface energy compares a situation with a surface to one without it, the calculated LDA and GGA E_s values should be corrected for by accounting for the truly nonlocal exchange-correlation effects. Very recently, one such correction scheme has been proposed for α-$Al_2O_3(0001)$, in which a correction term is added *a posteriori* to the calculated LDA and GGA values.[60] The lower part of Table IV shows the result of applying this correction term on our E_s values. As can be seen, the LDA and GGA values are now in very good agreement.

The observed discrepancy between the LDA and the GGA thus arises from the need to include truly nonlocal effects in exchange and correlation when dealing with surfaces. However, while these effects are important when calculating E_s, they are not significant when dealing with the *differences* between the E_s values of similar surfaces. The nonlocal effects should be very similar for similar surfaces and thus cancel out when looking at energy differences between similar surfaces. Thus, calculations of the energy gain from surface relaxation and comparisons of the stability of different surface terminations of the same crystal should yield accurate results. In addition, we have checked that our calculated LDOS for α-$Al_2O_3(0001)$ is not affected by the choice of functional. No significant difference in form is found between our calculated LDA and GGA LDOS, showing that our analysis of the surface electronic structure is not affected by the choice of functional.

Figure 7 shows the surface LDOS, before and after relaxation, obtained from our DFT-GGA calculations. For the unrelaxed surface [Fig. 7(a)], a partly filled surface state (SS), can be seen just above the Fermi energy E_F, of Al $3s+p_z$ and O $2p_z$ character. After relaxation [Fig. 7(b)], this SS is pushed up into the conduction band. This agrees with the previous tight-binding results of Godin *et al.*[51] and the DFT-LDA results of Verdozzi *et al.*[48] According to our calculations, the peak of this SS at the unrelaxed surface lies 2.8 eV under the bottom of the conduction band. In order to get a picture of the nature of this SS, we plot in Fig. 8 a real-space three-dimensional picture of the total density of states at the Fermi energy. A clear dangling-bond character of the SS can be seen, mainly localized on the surface Al atom but lying also on the surface O atoms.

The calculated DFT-GGA charge density can be integrated to yield a measure of the ionicity of the surface atoms. We perform this with the approach used in Ref. 5, in which the supercell is divided into Voronoi cells (a generalization of Wigner-Seitz cells) around each atom, such that a point **r** in the supercell belongs to the Voronoi cell around atom *i* if

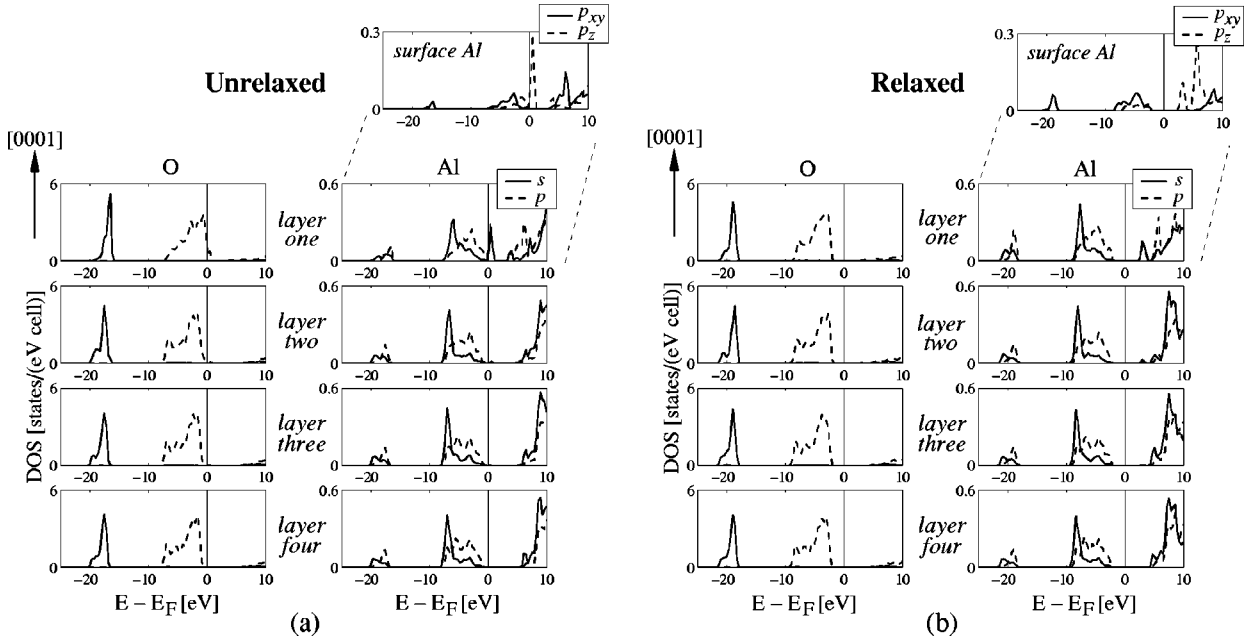

FIG. 7. Calculated local density of states (LDOS) from DFT-GGA on the unrelaxed (a) and relaxed (b) α-$Al_2O_3(0001)$ surfaces. The LDOS for the O and Al atoms in the top four surface layers (repeat units) are shown, projected onto atomic s and p valence orbitals. The pictures in the upper right corners show the LDOS for only the surface Al atom, projected onto valence p_{xy} and p_z orbitals.

$$\frac{|\mathbf{r}-\mathbf{R}_i|}{b_i} \leqslant \frac{|\mathbf{r}-\mathbf{R}_j|}{b_j}$$

for all atoms $j \neq i$, where b_i is the ionic radius of atom i, taken from the ''crystal radii'' tabulated by Shannon.[37] As pointed out in Ref. 5, this approach yields atomic charges that are in good agreement with other theoretical estimates[61,62] for bulk α-Al_2O_3.

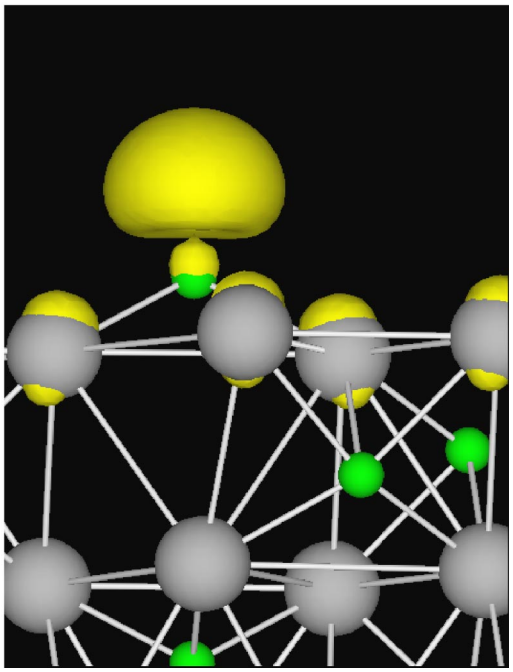

FIG. 8. (Color online) Real-space picture of the density of states at the Fermi energy (summed over all **k**) for the unrelaxed α-$Al_2O_3(0001)$ surface, calculated from DFT-GGA. Large balls are O atoms and small ones are Al atoms.

Such a calculation yields that before relaxation, the surface Al atom has a net atomic charge of $+2.67e$, that is, an excess of ≈ 0.1 electrons compared to the value obtained for a bulk Al atom ($\sim +2.78e$), while the O atoms in the two surface layers have as a whole lost approximately the same amount. This is presumably due to the fact that breaking the ionic Al–O bonds when creating the surface restores the electrons that were donated by the Al atoms, through these bonds, to the neighboring O atoms back to the Al atoms. Therefore, charge is restored to the surface Al ion, which has lost half of its nearest-neighbor O atoms, while charge is removed from the surface O ions, which have lost one of their nearest-neighbor Al atoms. This is reflected in our calculations by the presence of a partly filled SS band of dangling-bond character on the surface Al atoms and by the surface O valence bands crossing E_F, thus leaving empty states at the top of these bands [Figs. 7(a) and 8].

According to Brown's rule, Eq. (2) (using our calculated DFT-GGA Al–O bulk distances), each of the Al–O bonds broken in the crystal cleavage ''contains'' 0.40 electrons. However, it can be expected that charge redistributions take place through the remaining surface Al–O bonds, striving to restore the bulk ionicity of the surface ions and thus reduce the charge excess (deficit) of the surface Al (O) ions.

After relaxation, our calculated atomic charges show that the bulk ionicity is restored, which is consistent with our results of a bulklike LDOS for the relaxed surface [Fig. 7(b)].

B. κ-$Al_2O_3(001)$ and $(00\bar{1})$

The previous results on α-Al_2O_3 show the validity of our method for the description of the structure and bonding of

TABLE V. Calculated DFT-GGA E_{sep} values for all possible surface terminations of κ-$Al_2O_3(001)/(00\bar{1})$ (Fig. 6), before and after relaxation. The first two relaxed values correspond to only relaxing the (001) and the $(00\bar{1})$ surfaces of the slab, respectively. The third value is obtained by subtracting the two energy gains of these two relaxations from the unrelaxed value. The E_{sep} values obtained from our DFT-GGA calculations on α-$Al_2O_3(0001)$ are included for comparison.

Termination	Unrelaxed $E_{sep}(J/m^2)$	Relaxed $E_{sep}(J/m^2)$		
		Only (001)	Only $(00\bar{1})$	Total
1Al(I)	7.0	5.2	5.8	4.0
1O(I)	6.9	6.0	5.8	4.9
1O(II)	7.4	6.7	6.2	5.5
1Al(II)	9.5	7.5	7.5	5.5
2O(I)	8.5	7.6	8.1	7.2
2O(II)	9.7	8.1	8.9	7.3
2Al(I)	12.0	11.7	9.5	9.2
2Al(II)	11.5	11.3	9.8	9.6
3O(I)	13.6	10.6	13.3	10.3
3O(II)	14.4	11.5	13.8	10.9
α-$Al_2O_3(0001)$	7.2			3.2

alumina surfaces. Regarding the κ-$Al_2O_3(001)$ and $(00\bar{1})$ surfaces, the first question to address is the nature of the surface termination.

As discussed in Sec. II D, none of the κ-$Al_2O_3(001)/(00\bar{1})$ surface terminations that can be obtained from a cleavage of the κ-Al_2O_3 bulk structure is nonpolar, in Tasker's definition. Therefore, we calculate the E_{sep} value for all the ten possible cleavage terminations, shown in Fig. 6. The results are given in Table V. After relaxation of both the (001) and $(00\bar{1})$ faces of the slab for all ten terminations, the lowest E_{sep} value is found for termination 1Al(I). This is one of the two terminations with cleavage plane in the middle of an Al layer and thus most resemblant to the nonpolar α-$Al_2O_3(0001)$. As opposed to the other termination similar to α-$Al_2O_3(0001)$, 1Al(II), 1Al(I) has no Al^T in its immediate subsurface layers (see Fig. 6). This shows a lower stability for Al^T near the surface, compared to Al^O. Indeed, the other terminations having Al^T near the surface also show an instability of these Al^T units; during relaxation the surface O (Al) atoms that lie directly on top of second-layer Al (O) atoms undergo significant lateral displacements. This Al^T instability disappears, however, when a new layer of Al is put above these terminations. This result can be understood from Pauling's rules. As discussed in Sec. II C, the Al^T units are in the bulk stabilized by the presence of vacancy lines in the neighboring octahedral Al layers. Removal of these octahedral layers exposes the inherent instability of Al^T in Al_2O_3 structures, as expressed by Pauling's first rule and demonstrated by the stability of the α phase.

As discussed in Sec. II C, the same stabilizing interplay between Pauling's first and third rules seems to be at work in other metastable aluminas as well. Therefore, given the general applicability of Pauling's rules, there are good reasons to expect that this surface-Al^T instability is a common feature of metastable aluminas.

This applicability of Pauling's rules also gives clues on the stability of other surface geometries than those obtained by bulk-structure cleavage, conceivable, e.g., during a crystal-growth process. Structures having surface Al ions directly above second-layer Al ions would be less favorable due to Pauling's third rule. Also, change of the surface O layer in such a way that it creates additional Al^T in the second Al layer can be expected to be unfavorable due to Pauling's first rule. In cases with surface ions having a choice of several different positions that all satisfy Pauling's rules, it can be expected that these ions will prefer sites that maximize their mutual in-plane distances. This they do in order to minimize their electrostatic repulsion energy, a result that has also been found by Jennison and Bogicevic[14] in their study of thin Al_2O_3 layers. We notice, however, that the ten cleavage terminations considered by us above automatically satisfy most of these requirements (since they are directly derived from the bulk structure) and should therefore be the first-choice candidates for the κ-$Al_2O_3(001)/(00\bar{1})$ surface geometry.

The relaxation of the κ-$Al_2O_3(001)$ and $(00\bar{1})$ surfaces obtained for the 1Al(I) termination is described in Fig. 9 and Table VI. The asymmetry of the κ-Al_2O_3 bulk structure is evident in these relaxations. While at (001), there is a remarkably large 117% contraction of surface Al–O interlayer distance, yielding an O termination, at $(00\bar{1})$ there is "only" a 74% contraction. In both the cases, the strong inward relaxation can be understood in the same way as for α-$Al_2O_3(0001)$; the strong electrostatic attraction between Al and O and the loss of coordination of the surface Al pulls the Al ion towards the O layer. The open crystal structure allows a large relaxation while keeping the bond lengths intact.[51] The structure in κ-Al_2O_3 is even more open than in α-Al_2O_3, however, due to the vacancy lines in the second surface layer. Therefore, the surface Al ions can relax more deeply into these lines, still without noticeably altering their Al–O bond lengths.

The geometrical details of these atomic relaxations have been described in Ref. 12. Here, we comment in more detail on the obtained strong difference in relaxation between the two faces. As described in Ref. 12, this difference is due to the asymmetry of the Al^T units lying below the second surface-oxygen layer. While at (001), the Al ions directly beneath the second-layer Al-vacancy lines are Al^O and thus relatively free to relax into the bulk to accommodate for the inward relaxation of the surface Al ions, at $(00\bar{1})$ these Al ions are inverted Al^T (see Fig. 9). These atoms sit in top positions above the underlying O atoms and are thus less able to relax into the bulk. [Indeed, the Al^O (b_γ) directly beneath the surface Al of (001) relax 0.04 Å into the bulk, while the Al^T (c_β) directly beneath the surface Al of $(00\bar{1})$ remain still (see Table VI).] As a consequence, they cause a higher electrostatic repulsion on the surface Al ions, which therefore do not relax as fully as in the case of the (001)

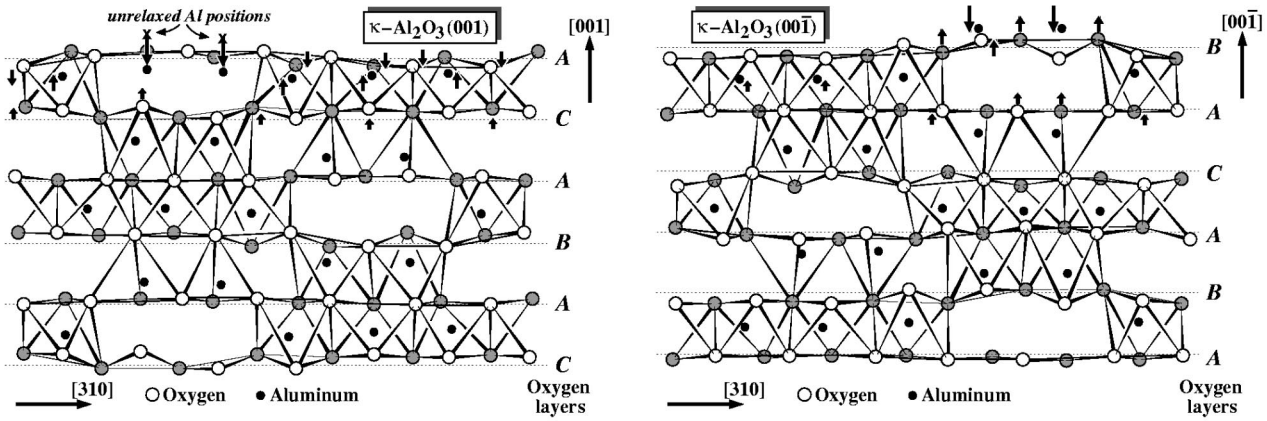

FIG. 9. Relaxation of the 1Al(I) κ-$Al_2O_3(001)$ and $(00\bar{1})$ surfaces, according to our DFT-GGA calculations. A slice of the atomic structure is shown, one coordination-polyhedron thick. ''Shaded'' O atoms lie behind ''open'' ones in the same layer. Solid lines show the Al coordination polyhedra. The major atomic movements during the relaxation are shown by the arrows.

surface. This causes the surface O ions to move outwards, in an attempt to further lower the electrostatic energy of the system. This outwards motion affects oxygen layers deep into the bulk, starting a ''cascade'' of small outwards O relaxations of about 0.01 Å at least as deep as ten O layers into the bulk, which is the largest amount of relaxed layers considered in our calculations. Indeed, even after relaxation of ten O layers, there still exists a potential gradient along [001] in the unrelaxed region of the slab (Fig. 10), implying that this outwards O relaxation continues even deeper. Estimates of this gradient yield, however, that it decays by $\approx 10\%$ for each new relaxed repeat unit that is added to the slab, showing that the relaxation will eventually decay to zero, if enough atomic layers are considered. [We have also checked that this gradient is not a mere effect of the (001) surface not having been relaxed in these calculations: a gradient is still present in slabs with thicker unrelaxed regions as well as in a slab in which all the atomic positions at *both* the surfaces have been set to their respective relaxed values.] We thus note that what at first appears to be only a subtle structural feature (the direction of the Al^T in the second surface layer) can, in fact, have a crucial and long-ranging effect on the surface stability and structure of a highly ionic crystal such as κ-Al_2O_3. This stresses the importance of using large enough cells when examining structural defects in aluminas and other highly ionic crystals.

The openness of the κ-Al_2O_3 structure is common to other metastable alumina phases. As discussed in Sec. II C, the presence of Al^T in the bulk allows several metastable alumina structures (κ, θ, γ, δ, η) to avoid face sharing between the Al coordination polyhedra, a fact that contributes to their structural stability according to Pauling's third rule. Thus, large vacancy regions, similar to those present in κ-Al_2O_3, can be expected to be present in these other phases as well. Indeed, the θ phase has even wider vacancy lines in its structure than κ-Al_2O_3.[38] Also, recent first-principles calculations show that the cation vacancies in the ideal cubic-spinel structures of γ-, η-, and δ-Al_2O_3 lie preferably on the octahedral sites.[6,63] Removal of any Al^O in the octahedral cation layer of the ideal spinel structure creates a large vacancy region in these structures as well. Thus, large vacancy regions are present in a number of different metastable alumina structures. In all cases, these are caused indirectly by the presence of Al^T in the structures. Therefore, it is plausible to assume that the strong surface relaxation predicted for κ-Al_2O_3 is a common feature of metastable aluminas, in which Al^T are present.

In this context, it is interesting to notice that a presence of abnormally coordinated Al ions (quasioctahedral and quasitrihedral) has been observed by Zhou and Snyder in bulk-structure studies of spinel aluminas.[38] However, Zhou and Snyder suggest that this is in effect caused by the high surface area of these phases and that these ions are in reality displaced Al^T lying in the surface region. It has been reported that the majority of the new surfaces created during the dehydroxylation of aluminum hydroxides to spinel alumina phases are (111) surfaces,[38] which have the same layer-by-layer Al/O close-packed structure as κ-$Al_2O_3(001)$/$(00\bar{1})$. Our results show, indeed, that very strong inward Al relaxations occur in the proximity of vacancy regions at close-packed surfaces and thus support the above picture.

We thus find that the most favorable surface termination for κ-$Al_2O_3(001)/(00\bar{1})$ is the one resembling that for the nonpolar α-$Al_2O_3(0001)$ surface. However, due to the unsymmetrical Al–O interlayer distances, all surface terminations of κ-Al_2O_3 should be polar, according to Tasker's definition (see Sec. II D). Yet, our calculated E_{sep} values for the 1Al(I) termination show no sign of divergence, as the slab thickness n is increased, which would be the case if the obtained surfaces were unstable. In Ref. 12 we show that in reality the 1Al(I) termination for κ-Al_2O_3 is nonpolar, by analyzing the calculated charge density in the slab and by applying Brown's definition of bond strength [Eq. (2)] on the κ-Al_2O_3 bulk structure. In the following, we repeat that analysis in more detail.

Table VII shows the net atomic charges calculated from our DFT-GGA charge densities with the Voronoi approach described in Sec. III A. The charges of the surface atoms at the unrelaxed and relaxed κ-$Al_2O_3(001)$ and $(00\bar{1})$ surfaces

TABLE VI. Relaxation data for the 1Al(I) κ-$Al_2O_3(001)$ and κ-$Al_2O_3(00\bar{1})$ surfaces, as obtained from our DFT-GGA calculations (see also Fig. 6).

	Interlayer distances (Å)			Atomic displacement	
	Bulk	Relaxed	Change		(Å)
(001) surface:					
$Al(b_\gamma)-O(A_\gamma)$	0.53	−0.40	−0.93	$Al(b_\gamma)$	−0.92
$O(A_\gamma)-O(A_\alpha)$	0.05	0.10	+0.05	$O(A_\gamma)$	+0.02
$O(A_\alpha)-O(A_\beta)$	0.06	0.21	+0.15	$O(A_\alpha)$	−0.03
$O(A_\beta)-Al(b_\beta^O)$	1.07	0.73	−0.34	$O(A_\beta)$	−0.18
$Al(b_\beta^O)-Al(b_\alpha^O)$	0.09	0.08	−0.01	$Al(b_\beta^O)$	+0.16
$Al(b_\alpha^O)-O(C_\alpha)$	0.85	0.89	+0.04	$Al(b_\alpha^O)$	+0.17
$O(C_\alpha)-O(C_\beta)$	0.06	0.20	+0.14	$O(C_\alpha)$	+0.12
$O(C_\beta)-O(C_\gamma)$	0.23	0.14	−0.09	$O(C_\beta)$	−0.02
$O(C_\gamma)-Al(b_\gamma^O)$	0.77	0.88	+0.11	$O(C_\gamma)$	+0.07
$Al(b_\gamma^O)-Al(c_\beta^T)$	0.79	0.72	−0.07	$Al(b_\gamma^O)$	−0.04
$Al(c_\beta^T)-O(A_\beta)$	0.53	0.56	+0.03	$Al(c_\beta^T)$	+0.03
$O(A_\beta)-O(A_\alpha)$	0.05	0.06	+0.01	$O(A_\beta)$	±0.00
$O(A_\alpha)-O(A_\gamma)$	0.06	0.02	−0.04	$O(A_\alpha)$	−0.01
$O(A_\gamma)-Al(c_\gamma^O)$	1.07	1.10	+0.03	$O(A_\gamma)$	+0.03
...			$<\pm 0.02$	...	$<\pm 0.01$
$(00\bar{1})$ surface:					
$Al(c_\beta)-O(B_\beta)$	0.77	0.20	−0.57	$Al(c_\beta)$	−0.39
$O(B_\beta)-O(B_\gamma)$	0.23	0.48	+0.25	$O(B_\beta)$	+0.19
$O(B_\gamma)-O(B_\alpha)$	0.06	−0.05	−0.11	$O(B_\gamma)$	−0.06
$O(B_\alpha)-Al(c_\alpha^O)$	0.85	0.94	+0.09	$O(B_\alpha)$	+0.05
$Al(c_\alpha^O)-Al(c_\gamma^O)$	0.09	−0.07	−0.16	$Al(c_\alpha^O)$	−0.05
$Al(c_\gamma^O)-O(A_\gamma)$	1.07	1.22	+0.15	$Al(c_\gamma^O)$	+0.11
$O(A_\gamma)-O(A_\alpha)$	0.06	0.01	−0.05	$O(A_\gamma)$	−0.04
$O(A_\alpha)-O(A_\beta)$	0.05	−0.06	−0.11	$O(A_\alpha)$	+0.02
$O(A_\beta)-Al(c_\beta^T)$	0.53	0.66	+0.13	$O(A_\beta)$	+0.13
$Al(c_\beta^T)-Al(b_\gamma^O)$	0.79	0.80	+0.01	$Al(c_\beta^T)$	±0.00
$Al(b_\gamma^O)-O(C_\gamma)$	0.77	0.77	±0.00	$Al(b_\gamma^O)$	−0.01
$O(C_\gamma)-O(C_\beta)$	0.23	0.21	−0.02	$O(C_\gamma)$	±0.00
$O(C_\beta)-O(C_\alpha)$	0.06	0.05	−0.01	$O(C_\beta)$	+0.02
$O(C_\alpha)-Al(b_\alpha^O)$	0.85	0.88	+0.03	$O(C_\alpha)$	+0.03
...			$<\pm 0.03$	Al: 0 − −0.01	
				O: +0.01 − +0.02	

are compared to the charges of the corresponding atoms in the bulk. Use of the valence-sum rule [Eq. (1)] on bulk κ-Al_2O_3, with Brown's bond-strength definition [Eq. (2)] and the bulk Al–O bond lengths obtained from our DFT-GGA calculations, yields bulk ionicities for the Al b_γ and c_β atoms of +2.91 and +2.82, respectively, which are in surprisingly good agreement with the DFT values. Therefore, Brown's bond strength should be a good measure of the actual amount of charge donated by an Al ion in the bulk to each of its neighboring O ions. This amount of charge depends on the Al–O distance; the larger the distance, the weaker the bond and consequently the smaller the charge transfer.

We can then calculate how much charge is transferred from the Al ions to the bulk O layer above and below,

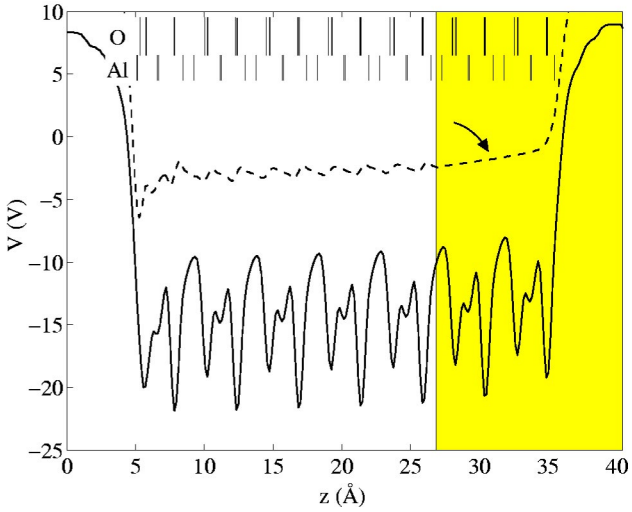

FIG. 10. (Color online) Plot of the xy-averaged total potential, as a function of z, in the largest slab considered by us for the relaxation of the κ-$Al_2O_3(00\bar{1})$ surface. The shaded region to the right shows the part of the slab kept fixed at bulk coordinates during the relaxation. The coordinate z runs along the [001] direction. Solid line: total potential in the relaxed slab. Dashed line: difference between the total potential in the relaxed slab and the total potential in bulk κ-Al_2O_3. The positions of the O and Al atoms are marked with the lines in the upper part of the figure. The arrow indicates the potential gradient still left in the unrelaxed part of the slab after relaxation.

respectively.[66] The Al^T transfers 0.69 electrons to the O layer above and 2.22 electrons to the O layer below. The large difference is due to the tetrahedral coordination, with only one Al–O bond to the layer above and three bonds to the layer below (see Fig. 11). The Al^O transfers 1.83 electrons to the layer above and 0.99 electrons to the layer below. Here the difference is due to the distortion of the octahedron, with a larger Al–O distance to the O layer below.

Now, cleavage of the bulk κ-Al_2O_3 structure involves breaking of Al–O bonds. It is then expected that the charge donated by the Al ions to the neighboring O ions through these bonds is restored to the Al ions, which then redistribute it to their remaining nearest-neighbor O atoms. Figure 11 shows schematically what happens when creating the 1Al(I) surfaces: 0.69 electrons are lost by the resulting $(00\bar{1})$ surface and "given back" to the (001) surface, while 0.99 electrons are transferred from (001) to $(00\bar{1})$. The result is that after crystal cleavage there is an excess of 0.30 electrons per Al atom at the $(00\bar{1})$ surface and a deficit of the same amount at (001), compared to the bulk situation. This is indeed the same amount of charge transfer obtained by summing up the DFT atomic charges (see Table VII).

As stated in Sec. II D, a Tasker-polar surface is unstable, due to the presence of a non-vanishing dipole moment perpendicular to the structural repeat unit used to build up the surface. Thus, a polar surface could be stabilized by transferring charge between the two surfaces of a slab in such a way that the destabilizing dipole moment is compensated by an equally large but opposite dipole. Such an analysis has been performed by a number of authors, most notably by

TABLE VII. Net charges (in units of electron charge) for the atoms in the surface layer of κ-$Al_2O_3(001)$ and $(00\bar{1})$, as obtained from our calculated DFT-GGA charge densities. The values for the atoms in the κ-Al_2O_3 bulk environment as well as at the unrelaxed (UR) and relaxed (R) surfaces are given (Refs. 64, 65).

Surface:	κ-$Al_2O_3(001)$					κ-$Al_2O_3(00\bar{1})$				
Atom:	O			Al		Al	O			
	(A_α)	(A_β)	(A_γ)	(b_γ^T)	Sum	(c_β^O)	(B_α)	(B_β)	(B_γ)	Sum
Bulk	−1.92	−1.87	−1.90	+2.89	−2.80	+2.78	−1.80	−1.79	−1.93	−2.74
UR	−1.84	−1.42	−2.13	+2.87	−2.52	+2.62	−1.90	−2.22	−1.58	−3.08
R	−1.80	−1.68	−1.88	+2.88	−2.48	+2.74	−1.88	−2.05	−1.78	−2.97 (Ref. 65)

Harding,[67] who allows an arbitrary number of atomic layers in the repeat unit, at arbitrary positions and with arbitrary charges. In his description, the dipole compensation is achieved by replacing the atomic plane on one side of the slab, having charge q_1, by a plane having charge αq_1 and by placing a new plane with charge $(1-\alpha)q_1$ at the other side of the slab. Assigning arbitrary charges q_i and coordinates r_i to each atomic plane i, the condition of dipole neutralization of such a slab yields then, according to Harding,

$$\alpha = 1 + \sum_{i=1}^{N} \frac{q_i r_i}{q_1 a},$$

where N is the number of atomic planes in the repeat unit and a is the height of the repeat unit.

Insertion of our DFT-GGA bulk interlayer distances (Fig. 6) and of the charges of each atom obtained from our DFT-GGA bulk charge density yields that a charge transfer of 0.69 electrons is needed per unit cell, that is, per two Al atoms, to neutralize the polarity of the κ-$Al_2O_3(001)/(00\bar{1})$ surface system.

The fact that the charge transfers obtained from our DFT calculations and from Harding's formula agree implies that, in reality, this κ-$Al_2O_3(001)/(00\bar{1})$ surface termination is *nonpolar*. More importantly, this shows that the charge transfer needed to stabilize the surface is provided for in a natural way. Obtaining it through an actual flow of charge through the slab would be quite difficult, considering the wide band gap of the material. Here it arises as a natural consequence of the intrinsic charge asymmetry of bulk κ-Al_2O_3. In other words, Tasker's rule is too simple a tool to describe the surface stability of low-symmetry crystals such as κ-Al_2O_3. Only by going beyond his ideal, fully ionic, and point-charge assumptions, is it possible to properly analyze the system.

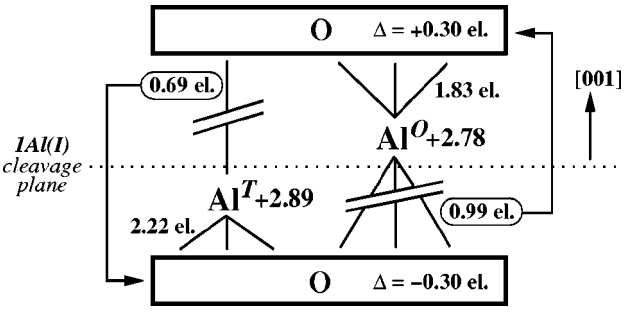

FIG. 11. A schematic picture of the charge transfer taking place when breaking the Al–O bonds during the creation of the 1Al(I) termination of κ-$Al_2O_3(001)/(00\bar{1})$. The Al ionicities are those calculated from our DFT-GGA bulk charge density (Table VII), while the electron amount in each group of Al–O bonds is given by summing up the corresponding values of Brown's bond strength [Eq. (2)].

Figure 12 shows the calculated LDOS for the atomic layers near the κ-$Al_2O_3(001)$ and $(00\bar{1})$ surfaces, before and after relaxation. Before relaxation, there are an Al SS at the Fermi energy E_F and a crossing of E_F by the O valence band, at both surfaces. This is similar to the unrelaxed α-$Al_2O_3(0001)$ surface (see Sec. III A). However, as shown above, at the κ-$Al_2O_3(001)$ surface, there is a deficit of electronic charge, while at κ-$Al_2O_3(00\bar{1})$ there is an excess of charge. Thus, after relaxation, the $(00\bar{1})$ surface is not able to restore full ionicity and retains a partly filled SS at the surface. The (001) surface, on the other hand, retains a partly empty O valence band. These surface states are thus necessary to accomodate the charge transfer.

We now analyze in more detail the electronic transfers taking place during the creation of the 1Al(I) κ-Al_2O_3 surfaces. As can be seen from Table VII, the electron deficit at the (001) surface is mainly localized around the O A_β atoms and also, although to a smaller degree, around the O A_α atoms. These are the nearest-neighbor O atoms to the Al c_β atom, which has been removed in the creation of the (001) surface. This agrees with our analysis above; the breaking of the Al c_β−O bonds has deprived these O atoms of the electrons donated to them by the Al c_β atoms. The O A_β atoms are especially affected by this, having two Al c_β atoms as nearest neighbors, while the O A_α atoms have only one nearest-neighbor Al c_β atom. At the same time, before relaxation, the surface O A_γ atoms have an excess of electrons. This is due to the breaking of the bond between the Al b_γ atom and the O B_γ atoms at the $(00\bar{1})$ surface. The charge restored to the Al b_γ atom after breaking of this bond is redistributed to the remaining nearest-neighbor O atoms: the two A_γ and one A_α atoms at the (001) surface.

Thus, before relaxation, the atomic charges are a direct consequence of the Al–O bond breaking. After relaxation, we see (Table VII) that the charges tend to redistribute between the surface O atoms. In particular, nature strives to restore the bulk ionicity of the O A_γ atoms, which have kept the atomic environment of the bulk. Charge is transferred

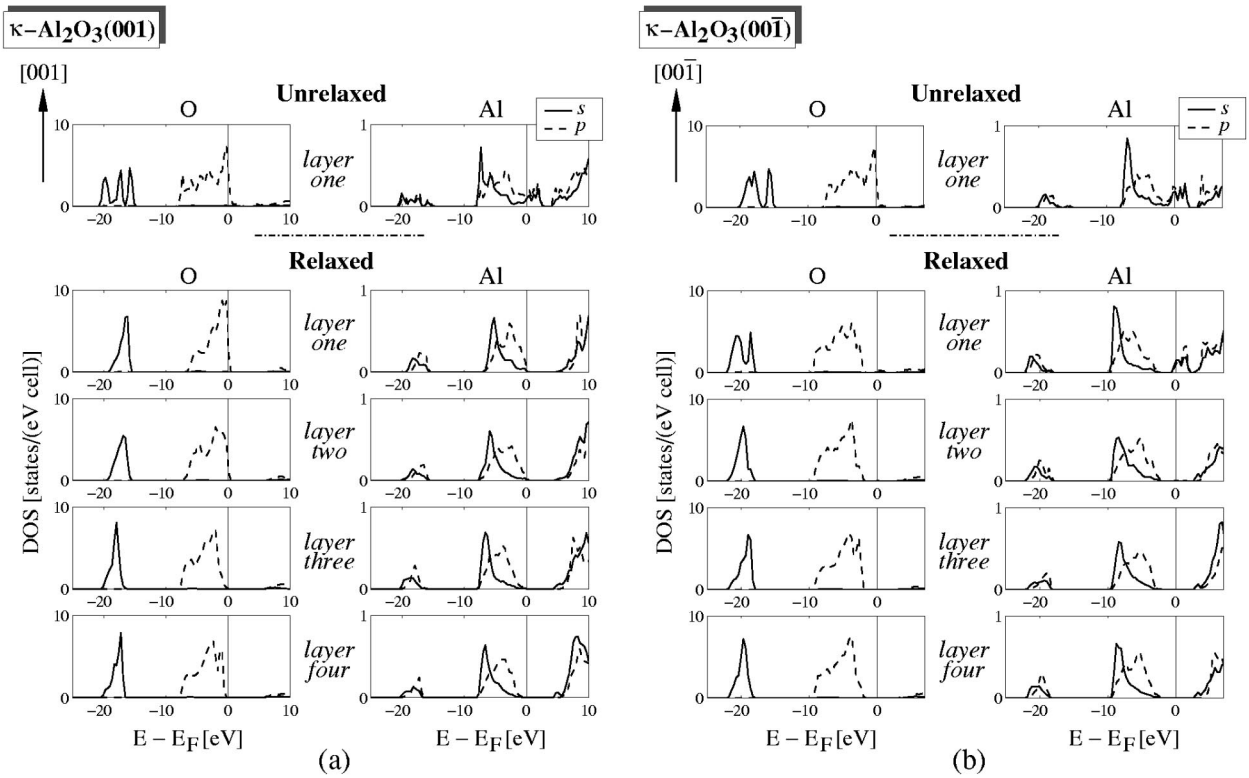

FIG. 12. Calculated local density of states (LDOS) from DFT-GGA, projected onto atomic *s* and *p* orbitals, for the O and Al atoms in the four (one) outermost layers of the relaxed (unrelaxed) κ-$Al_2O_3(001)$ (a) and $(00\bar{1})$ (b) surfaces at the 1Al(I) termination.

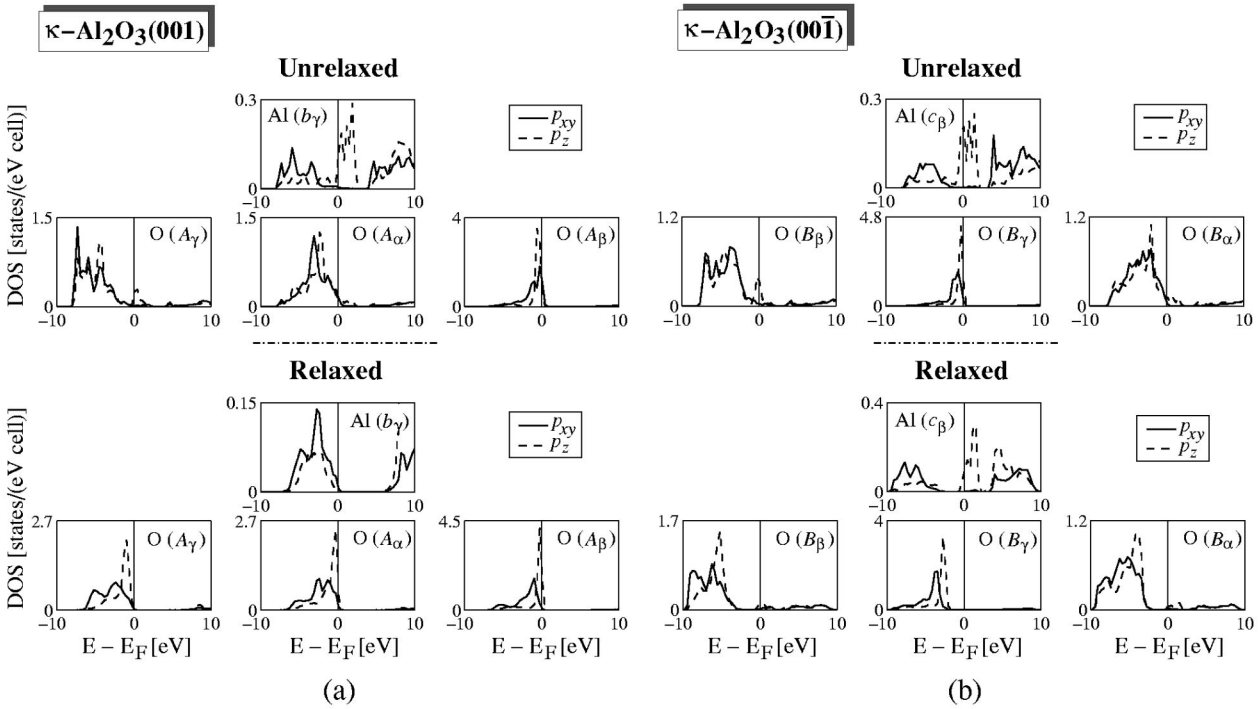

FIG. 13. Calculated local density of states (LDOS) from DFT-GGA, projected onto atomic p_{xy} and p_z orbitals, for each of the Al and O atoms in the outermost layer of the unrelaxed and relaxed κ-$Al_2O_3(001)$ (a) and $(00\bar{1})$ (b) surfaces at the 1Al(I) termination. Each of the different surface atoms is denoted by the position notation of Fig. 2.

from O A_γ to the strongly "undercharged" O A_β. The partial LDOS of Fig. 13 shows that this corresponds to the suppression of a partially-filled SS at O A_γ and the elimination of empty p_{xy} states at O A_β. After relaxation, the electron deficit at O A_β and A_α corresponds to empty p_z states at these atoms.

At $(00\bar{1})$ we see, in analogy to (001), an electron deficit at the O B_γ atom, which has lost its nearest-neighbor Al b_γ atom, and an electron excess at the O B_β and O B_α atoms, which receive the electrons left by the broken bonds between Al c_β and the O A_β and O A_α atoms at the (001) surface. However, here also an excess of electrons at the Al c_β atom is found. This is due to the overall excess of 0.30 electrons per Al atom at the $(00\bar{1})$ surface. Similar to what happens at the (001) surface, relaxation of the $(00\bar{1})$ surface strives to restore the bulk ionicity of the surface atoms by transfering charge away from the "overcharged" region around the O B_β, Al c_β, and O B_α atoms. However, the overall excess of electrons at the surface makes this redistribution incomplete, leaving an excess of electrons in the region surrounding the surface Al c_β atoms. This can be seen more clearly in Fig. 13. The relaxation succeeds in filling the empty states at the top of the O B_γ valence band but fails in completely eliminating the partially filled surface states at the other surface atoms. After relaxation, the $(00\bar{1})$ surface is thus left with a partially filled surface-state band, of predominantly s and p_z character, that is mainly localized around the Al c_β atoms but also, to a smaller extent, around the nearest-neighbor O B_β and O B_α atoms.

Figure 14 shows the band structure calculated for a κ-Al_2O_3 slab with both (001) and $(00\bar{1})$ surfaces relaxed. The surface state at $(00\bar{1})$, crossing the Fermi energy E_F, is clearly visible. Furthermore, the surface state has a paraboliclike form in the [100] direction, that is, along the zigzag line of the surface Al atoms, and is almost flat along [010], that is, in the direction normal to the surface Al lines. The effective mass of the electrons along [100] is calculated to be $\approx 1.4 m_e$, where m_e is the electron mass, at the Fermi energy (due to a misprint, this value was erroneously given as $0.14\, m_e$ in Ref. 12). This indicates a rather good dispersion of the surface state, implying a relatively good mobility along [100] for these surface electrons.

In Fig. 15, the calculated Kohn-Sham wave function corresponding to this surface state, at $\mathbf{k}_F$, is plotted in real space. The state is clearly localized mainly on the surface Al atoms. The smaller localization around the nearest-neighbor O atoms is also evident. However, the picture shows clearly that there is no coupling between the O and the Al electrons in this state.

Thus, this surface state has the character of a one-dimensional electron gas localized on the surface [100] zigzag line of Al atoms. Such a peculiar low-dimensional electron gas can be expected to have very interesting, experimental as well as theoretical, properties. Investigations are currently being conducted to further understand these properties.[68]

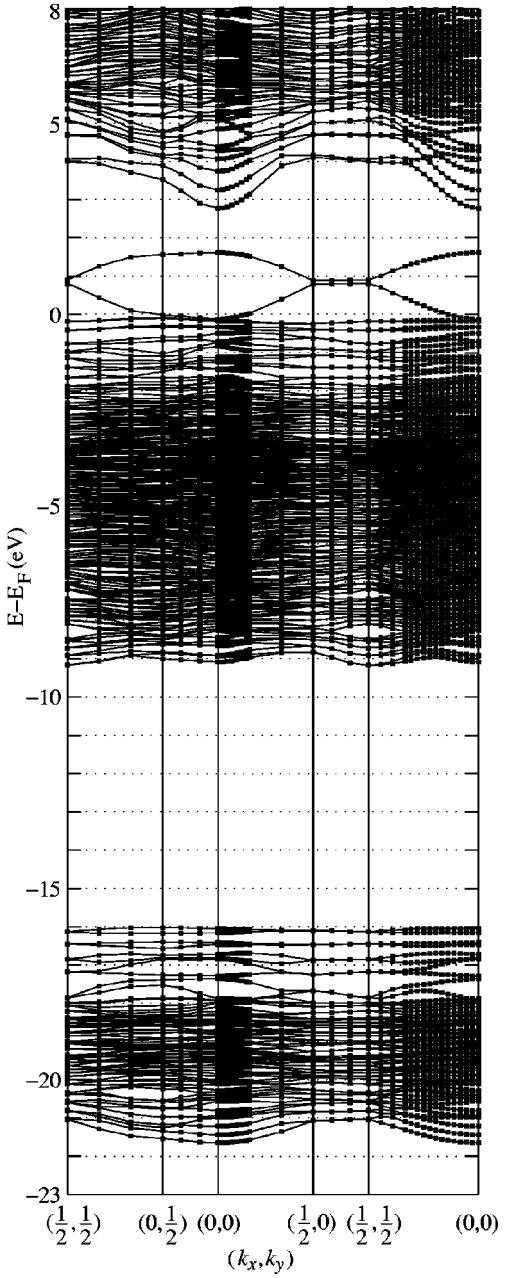

FIG. 14. Calculated band structure from DFT-GGA for a slab of κ-Al_2O_3 with relaxed (001) and $(00\bar{1})$ surfaces at the 1Al(I) termination. The **k**-point values are given relative to the two-dimensional Brillouin zone. Energies are relative to the Fermi energy E_F.

Finally, it is interesting to notice that metallic surface states also appear when cleaving the κ-Al_2O_3 crystal through (001) planes other than the one that yields the 1Al(I) termination. In fact, for *all* the ten possible cleavage terminations (Fig. 6), our calculated LDOS's show (after relaxation) a metallic surface state centered around surface Al atoms on one side and a crossing of the O valence band across E_F on the other side. Apparently, the charge asymmetry along [001] in κ-Al_2O_3 manifests itself independently of the choice of (001) cleavage plane. This confirms the picture of the metallic surface state of κ-$Al_2O_3(001)/(00\bar{1})$ being a

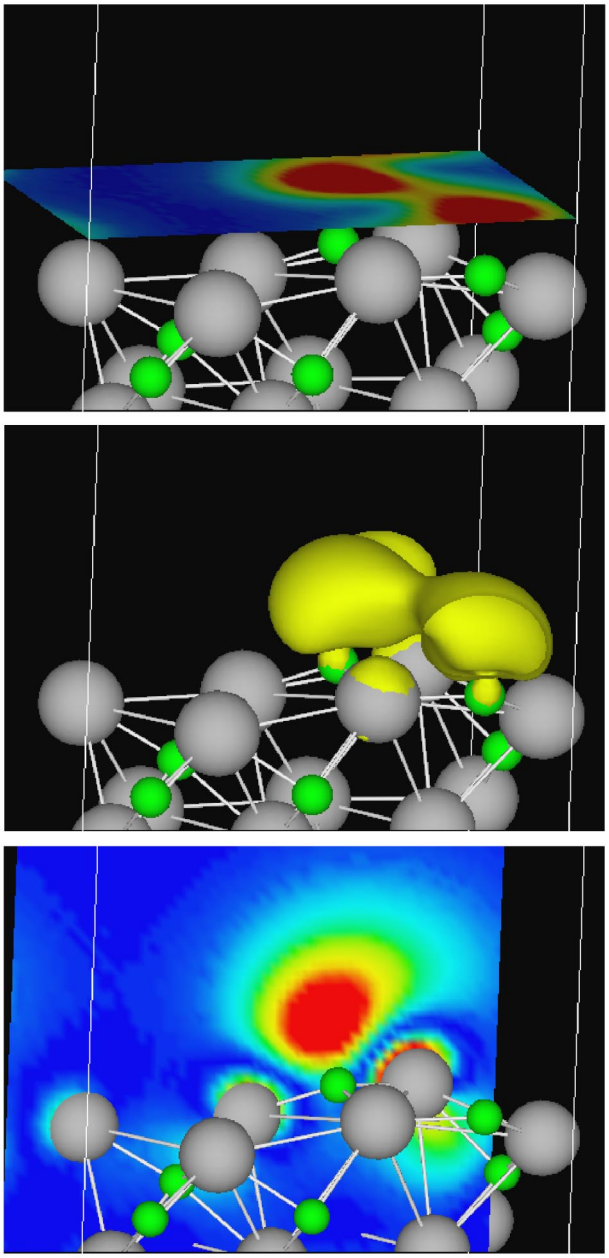

FIG. 15. (Color online) Real-space picture of the density of states corresponding to the surface state of the relaxed κ-$Al_2O_3(00\bar{1})$ surface at $\mathbf{k}=\mathbf{k}_F$, calculated from DFT-GGA. Large balls are O atoms and small ones are Al atoms. Only one unit cell (drawn with thin white lines) of the κ-Al_2O_3 surface is shown.

natural consequence of the charge asymmetry in bulk κ-Al_2O_3 (which in turn arises from the low symmetry of the κ-Al_2O_3 bulk structure together with its high ionicity and its large band gap, which prevents screening). The surface metallicity is thus not caused by the particular choice of cleavage plane.

IV. CONCLUSIONS

This study of the surface atomic and electronic structures of the metastable κ phase of alumina reveals unexpected features of the surface stability and bonding of this relatively complex and highly ionic crystal. In particular, a one-dimensional metallic surface state at the κ-$Al_2O_3(00\bar{1})$ surface is predicted to be present. If manufacturable, it can provide an important testing ground for theories on low-dimensional systems and exhibit technologically interesting properties connected with adsorption and catalysis. An experimental study of this one-dimensional electron gas is thus highly desirable. In separate papers, its robustness and Luttinger-liquid characteristics are explored.[69]

Generally, the limitations of point-charge models for describing low-symmetry complex ionic crystals are discussed. It is necessary to augment such descriptions, such as Tasker's rule, with more extended models that include more of the quantum-mechanical treatment. The present study shows that the energetically most favorable κ-$Al_2O_3(001)/(00\bar{1})$ cleavage surface termination is, in reality, nonpolar, despite the fact that a direct use of Tasker's rule yields a clear polar classification. In this context, we show that Brown's valence-sum rule (an extension of Pauling's second rule) is an excellent tool for studying the charge distribution in low-symmetric ionic crystals, yielding results that are in good quantitative agreement with those obtained from the first-principles DFT calculations.

In the field of metastable aluminas, important understanding is gained regarding the stability of their surfaces. The present results, generalizable through Pauling's rules, can be used to better understand the surface and bulk structures of the elusive metastable aluminas. In particular, we find strong relaxation effects whenever open-structured surfaces are exposed. In the presently studied system, the κ-$Al_2O_3(001)$ surface is predicted to undergo a huge inward relaxation, with a 117% contraction of the top Al–O interlayer distance, at UHV conditions yielding an O termination after relaxation [in contrast to the α-$Al_2O_3(0001)$ surface]. This result is understood in terms of simple electrostatic arguments, based on the fact that the presence of tetrahedrally coordinated Al atoms (Al^T) in the bulk structure creates large vacancy regions in the structure because of Pauling's third rule. The result is thus generalizable to other metastable alumina phases. For example, our result confirms the explanation proposed by Zhou and Snyder[38] for the observed presence of abnormally coordinated Al ions in bulk-structure studies of the spinel-structured aluminas (γ, η, and δ).

Further, we show that, again because of the openness of the structure, long-ranging electrostatic effects have crucial importance for the surface structure and stability of highly ionic crystals such as κ-Al_2O_3. At the κ-$Al_2O_3(00\bar{1})$ surface, we find that the strong inward relaxation of the top Al layer [observed at the (001) surface] is strongly hindered by the presence of Al^T units in the third surface layer. Thus, there is only a 74% contraction of the top Al–O interlayer distance at $(00\bar{1})$, leaving an Al termination. This stresses the importance of using large enough cells when calculating effects arising from structural defects in aluminas and other highly ionic crystals.

Also, we find that the Al^T, when exposed in a near-surface region, become unstable with respect to Al^O, a fact in agreement with Pauling's rules and thus also generalizable to metastable aluminas.

Finally, we note that this is the first study from first principles on the atomic structure and stability of a κ-Al_2O_3 surface. It yields essential information for understanding and further studying the properties of the chemical-vapor deposited (CVD) coatings of κ-Al_2O_3 on cemented-carbide cutting tools. In particular, it shows the non-equivalence of the (001) and $(00\bar{1})$ surfaces. This difference should have dramatic importance for the mechanism lying behind the complex CVD growth process. Our results provide clues for how to determine experimentally which of the surfaces is the actual growth direction of CVD κ-Al_2O_3.

ACKNOWLEDGMENTS

We thank Lennart Bengtsson for support and optimization of the DACAPO 1.30 computer code and Mats Halvarsson for inspiring and valuable discussions. Financial support from the Swedish Foundation for Strategic Research via Materials Consortium No. 9 and computer use at UNICC (Unix Numeric Intensive Calculations at Chalmers), Chalmers University of Technology, Göteborg (Sweden), and at PDC (Center for Parallel Computers) at KTH (Kungliga Tekniska Högskolan), Stockholm (Sweden) are gratefully acknowledged.

[1] I. Levin and D. Brandon, J. Am. Ceram. Soc. **81**, 1995 (1998).
[2] L. D. Hart, *Alumina Chemicals: Science and Technology Handbook* (The American Ceramic Society, Ohio, 1990).
[3] C. Misra, *Industrial Alumina Chemicals* (American Chemical Society, Washington, DC, 1986).
[4] M. Wilson, M. Exner, Y.-M. Huang, and M.W. Finnis, Phys. Rev. B **54**, 15 683 (1996).
[5] Y. Yourdshahyan, C. Ruberto, M. Halvarsson, L. Bengtsson, V. Langer, B.I. Lundqvist, S. Ruppi, and U. Rolander, J. Am. Ceram. Soc. **82**, 1365 (1999).
[6] C. Wolverton and K.C. Hass, Phys. Rev. B **63**, 024102 (2001).
[7] H.-L. Gross and W. Mader, Chem. Commun. (Cambridge) **1997**, 55 (1997).
[8] B. Ollivier, R. Retoux, P. Lacorre, D. Massiot, and G. Férey, J. Mater. Chem. **7**, 1049 (1997).
[9] L. Smrčok, V. Langer, M. Halvarsson, and S. Ruppi, Z. Kristallogr. **216**, 409 (2001).
[10] P. Hohenberg and W. Kohn, Phys. Rev. **136**, B864 (1964); W. Kohn and L.J. Sham, *ibid.* **140**, A1133 (1965).
[11] B.I. Lundqvist, A. Bogicevic, K. Carling, S.V. Dudiy, S. Gao, J. Hartford, P. Hyldgaard, N. Jacobson, D.C. Langreth, N. Lorente, S. Ovesson, B. Razaznejad, C. Ruberto, H. Rydberg, E. Schröder, S.I. Simak, G. Wahnström, and Y. Yourdshahyan, Surf. Sci. **493**, 253 (2001).
[12] C. Ruberto, Y. Yourdshahyan, and B.I. Lundqvist, Phys. Rev. Lett. **88**, 226101 (2002).
[13] M. Halvarsson and S. Vuorinen, Surf. Coat. Technol. **76-77**, 287 (1995).
[14] D.R. Jennison and A. Bogicevic, Surf. Sci. **464**, 108 (2000).
[15] M. Bäumer and H.-J. Freund, Prog. Surf. Sci. **61**, 127 (1999).
[16] S. Tehrani, B. Engel, J.M. Slaughter, E. Chen, M. DeHerrera, M. Durlam, P. Naji, R. Whig, J. Janeski, and J. Calder, IEEE Trans. Magn. **36**, 2752 (2000).
[17] P.J. Eng, T.P. Trainor, G.E. Brown, Jr., G.A. Waychunas, M. Newville, S.R. Sutton, and M.L. Rivers, Science (Washington, DC, U.S.) **288**, 1029 (2000).
[18] C. Niu, K. Shepherd, D. Martini, J. Tong, J.A. Kelber, D.R. Jennison, and A. Bogicevic, Surf. Sci. **465**, 163 (2000); S.A. Chambers, T. Droubay, D.R. Jennison, and T.R. Mattsson, Science (Washington, DC, U.S.) **297**, 827 (2002).
[19] B. Hammer *et al.*, (unpublished).
[20] J.P. Perdew, J.A. Chevary, S.H. Vosko, K.A. Jackson, M.R. Pederson, D.J. Singh, and C. Fiolhais, Phys. Rev. B **46**, 6671 (1992).
[21] J.P. Perdew and A. Zunger, Phys. Rev. B **23**, 5048 (1981).
[22] D. Vanderbilt, Phys. Rev. B **41**, 7892 (1990).
[23] N. Troullier and J.L. Martins, Phys. Rev. B **43**, 1993 (1991) for oxygen; G.B. Bachelet, D.R. Hamann, and M. Schlüter, *ibid.* **26**, 4199 (1982) for aluminum.
[24] H.J. Monkhorst and J.D. Pack, Phys. Rev. B **13**, 5188 (1976).
[25] L. Bengtsson, Phys. Rev. B **59**, 12 301 (1999).
[26] Y. Yourdshahyan and B. I. Lundqvist (unpublished).
[27] M. Halvarsson, V. Langer, and S. Vuorinen, Surf. Coat. Technol. **76–77**, 358 (1995).
[28] Y. Yourdshahyan, C. Ruberto, L. Bengtsson, and B.I. Lundqvist, Phys. Rev. B **56**, 8553 (1997).
[29] W.E. Lee and K.P.D. Lagerlof, J. Electron Microsc. Tech. **2**, 247 (1985).
[30] T. Yokokawa and O.J. Kleppa, J. Phys. Chem. **68**, 3246 (1964).
[31] L. Pauling and S.B. Hendricks, J. Am. Chem. Soc. **47**, 781 (1925).
[32] M. Halvarsson, Ph. D. thesis, Chalmers University of Technology, Göteborg, Sweden, 1994.
[33] L. Pauling, J. Am. Chem. Soc. **51**, 1010 (1929); L. Pauling, *The Nature of the Chemical Bond*, 3rd ed. (Cornell University, Ithaca, New York, 1960), pp. 396–400.
[34] A coordinated polyhedron of anions is formed about each cation, the cation-anion distance being determined by the sum of the cation and anion radii and the coordination number of the cation by the cation-to-anion radius ratio. A ratio between 0.225 and 0.414 implies a tetrahedral cation coordination, while a ratio between 0.414 and 0.732 implies an octahedral coordination.
[35] In a stable ionic structure the electric charge of each anion, with changed sign, is exactly or nearly equal to the sum of the strengths of the electrostatic bonds to it from the adjacent cations. The electrostatic bond strength is equal to the cation charge divided by the cation coordination number.
[36] The existence of shared edges, and particularly of shared faces, between two cation polyhedra in a coordinated structure decreases its stability, due to the enhanced cation-cation electrostatic repulsion.

[37] R.D. Shannon, Acta Crystallogr., Sect. A: Cryst. Phys., Diffr., Theor. Gen. Crystallogr. **32**, 751 (1976).
[38] R.-S. Zhou, R.L. Snyder, Acta Crystallogr., Sect. B: Struct. Sci. **47**, 617 (1991).
[39] I.D. Brown, Acta Crystallogr., Sect. B: Struct. Sci. **48**, 553 (1992); I.D. Brown and D. Altermatt, *ibid.* **41**, 244 (1985).
[40] V.S. Urusov, Acta Crystallogr., Sect. B: Struct. Sci. **51**, 641 (1995); J. K. Burdett, *Chemical Bonding in Solids* (Oxford University Press, New York, 1995), pp. 202–5.
[41] P.W. Tasker, J. Phys. C **12**, 4977 (1979).
[42] P.W. Tasker, Adv. Ceram. **10**, 176 (1984).
[43] See, C. Noguera, J. Phys.: Condens. Matter **12**, R367 (2000) for a review on the stability of polar oxide surfaces.
[44] J.C. Boettger, Phys. Rev. B **49**, 16 798 (1994).
[45] V. Fiorentini and M. Methfessel, J. Phys.: Condens. Matter **8**, 6525 (1996).
[46] J.G. Gay, J.R. Smith, R. Richter, F.J. Arlinghaus, and R.H. Wagoner, J. Vac. Sci. Technol. A **2**, 931 (1984).
[47] J.C. Boettger, Phys. Rev. B **53**, 13 133 (1996).
[48] C. Verdozzi, D.R. Jennison, P.A. Schultz, and M.P. Sears, Phys. Rev. Lett. **82**, 799 (1999).
[49] D.J. Siegel, Louis G. Hector, Jr., and J.B. Adams, Phys. Rev. B **65**, 085415 (2002).
[50] J.R.B. Gomes, F. Illas, N.C. Hernandez, A. Marquez, and J.F. Sanz, Phys. Rev. B **65**, 125414 (2002).
[51] T.J. Godin and J.P. LaFemina, Phys. Rev. B **49**, 7691 (1994).
[52] J. Guo, D.E. Ellis, and D.J. Lam, Phys. Rev. B **45**, 13 647 (1992).
[53] S. Blonski and S.H. Garofalini, Surf. Sci. **295**, 263 (1993).
[54] I. Batyrev, A. Alavi, and M.W. Finnis, Faraday Discuss. **114**, 33 (1999).
[55] R. Di Felice and J.E. Northrup, Phys. Rev. B **60**, R16 287 (1999).
[56] X.-G. Wang, A. Chaka, and M. Scheffler, Phys. Rev. Lett. **84**, 3650 (2000).
[57] P.D. Tepesch and A.A. Quong, Phys. Status Solidi B **217**, 377 (2000).
[58] H. Rydberg, B.I. Lundqvist, D.C. Langreth, and M. Dion, Phys. Rev. B **62**, 6997 (2000).
[59] K. Carling, G. Wahnström, T.R. Mattsson, A.E. Mattsson, N. Sandberg, and G. Grimvall, Phys. Rev. Lett. **85**, 3862 (2000).
[60] A.E. Mattsson and D.R. Jennison, Surf. Sci. **520**, L611 (2002).
[61] C. Sousa, F. Illas, and G. Pacchioni, J. Chem. Phys. **99**, 6818 (1993).
[62] W.Y. Ching and Yong-Nian Xu, J. Am. Ceram. Soc. **77**, 404 (1994).
[63] G. Gutiérrez, A. Taga, and B. Johansson, Phys. Rev. B **65**, 012101 (2001).
[64] It should be noted that small variations of ~0.01 electrons occur in the calculated charges of each atom, due to the finite nature of the sampling of the DFT charge density in real space (the distance between adjacent sampling points being ~0.15 Å, i.e., ~0.9% of the shortest Al–O distance). The values of Table VII should therefore be regarded to have such an accuracy.
[65] A charge transfer of ~0.05 electrons per Al atom occurs from first to second $(00\overline{1})$ O layer during relaxation and does not appear, therefore, in Table VII. The total charge sum at the relaxed $(00\overline{1})$ surface is therefore in reality $-2.97-0.05=-3.02$.
[66] We implicitly adopt the convention here of looking at the κ-Al_2O_3 structure with the [001] direction defined ''upwards,'' as in Figs. 6 and 11.
[67] J.H. Harding, Surf. Sci. **422**, 87 (1999).
[68] B. Razaznejad, C. Ruberto, N. Jacobson, P. Hyldgaard, and B. I. Lundqvist (unpublished).
[69] B. Razaznejad, C. Ruberto, P. Hyldgaard, and B. I. Lundqvist, Surf. Sci. (to be published); Phys. Rev. Lett. (to be published).